

Univerzita Karlova v Praze

Matematicko-fyzikální fakulta

DIPLOMOVÁ PRÁCE



Bc. Michal Roskot

Identifikace částic v experimentu COMPASS s pomocí technologie čerenkovských detektorů

Katedra fyziky nízkých teplot

Vedoucí diplomové práce: M.Sc. Michael Finger, CSc.

Studijní program: Fyzika

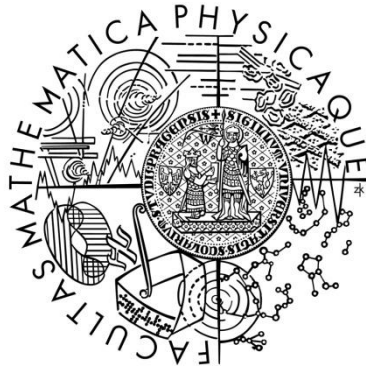
Studijní obor: Učitelství fyziky-matematiky pro střední školy

Praha 2015

Charles University in Prague

Faculty of Mathematics and Physics

MASTER THESIS



Bc. Michal Roskot

Particle Identification using Ring Cherenkov Detector Technology at COMPASS Experiment

Department of Low – Temperature Physics

Supervisor of the master thesis: M.Sc. Michael Finger, CSc.

Study programme: Physics

Specialization: Training Teachers of Physics
and Mathematics at Higher Secondary Schools

Prague 2015

At this point I would like to thank my supervisor Michael Finger for his expert advice, his kindness and patience. I want to thank Miroslav Finger for his overall support and for opportunity to participate on the COMPASS experiment. Many thanks belong to members of the COMPASS RICH group and in particular to my colleagues M. Bodlák, M. Krištof, J. Nový, M. Slunečka and L. Steiger for the preparation and realization of the 2014 year THGEM test experiments at CERN. Finally, I would like to thank Jan Šperling for language proofreading.

I declare that I carried out this master thesis independently, and only with the cited sources, literature and other professional sources.

I understand that my work relates to the rights and obligations under the Act No. 121/2000 Coll., the Copyright Act, as amended, in particular the fact that the Charles University in Prague has the right to conclude a license agreement on the use of this work as a school work pursuant to Section 60 paragraph 1 of the Copyright Act.

In Prague date 27. 6. 2015

signature

Název práce: Identifikace částic v experimentu COMPASS s pomocí technologie čerenkovských detektorů

Autor: Bc. Michal Roskot

Katedra / Ústav: Katedra fyziky nízkých teplot

Vedoucí diplomové práce: M.Sc. Michael Finger, CSc., Katedra fyziky nízkých teplot

Konzultant: prof. Ing. Miroslav Finger, DrSc.

Abstrakt: Diplomová práce je věnována vývoji detektoru pro identifikaci částic COMPASS RICH-1, který se nachází ve výzkumném centru Evropské organizace pro jaderný výzkum (CERN). K identifikaci částic je užito Čerenkovovo záření, jehož fyzikální podstata je společně s principy detekce v práci popsána. Současným cílem vývoje detektoru je výměna mnoha drátových komor (MWPC) v periferních částech detekční plochy za nově vyvíjené fotonové detektory založené na Micro-Megas a THGEM technologií tak, aby byla zaručena jedno-fotonová detekce. Pro tyto účely byl vytvořen zkušební detektor. Výsledky testování tohoto detektoru jsou v práci představeny.

Klíčová slova: Částicová identifikace, RICH detektor, THGEM detektor

Title: Particle Identification using Ring Cherenkov Detector Technology at COMPASS Experiment

Author: Bc. Michal Roskot

Department / Institute: Department of Low Temperature Physics

Supervisor of the master thesis: M.Sc. Michael Finger, CSc., Department of Low Temperature Physics

Consultant: prof. Ing. Miroslav Finger, DrSc.

Abstract: The presented thesis is dedicated to particle identification in COMPASS RICH-1 experiment which is located in European Organization for Nuclear Research (CERN). For particle identification Cherenkov radiation is used, which is described in the thesis together with detection principles. Current aim in detector upgrade is replacing a part of Multi Wire Proportional Chambers (MWPC) in peripheral regions of the detection surface by a suitable photon detector so as to guarantee one-photon detection. For this purpose the hybrid photon detector based on THGEM and MicroMegas technologies was developed. The hybrid detector test results are presented in the thesis.

Keywords: Particle identification, RICH detector, THGEM detector

Contents

Introduction.....	1
1 The COMPASS experiment in CERN.....	3
2 Cherenkov radiation	5
2.1 Description.....	5
2.2 Historical progress.....	5
2.3 Derivations.....	6
2.3.1 Classical derivation.....	6
2.3.2 Electrodynamics derivation.....	11
2.3.3 Quantum mechanics derivation	18
2.4 Some applications	21
2.5 Ring Imaging Cherenkov detectors.....	22
2.5.1. Cherenkov light imaging – basic formulas	22
2.5.2. Ring Imaging Cherenkov detector – the basis	23
3 COMPASS RICH-1.....	25
3.1 Experimental arrangement.....	25
3.1.1 Gas vessel.....	26
3.1.2 Focusing optics.....	27
3.1.3 Detection system	27

3.2	Detector upgrade.....	28
4	The hybrid photon detector based on THGEM and MicroMegas	33
4.1	The MicroMegas detector.....	33
4.2	The THGEM development	35
4.3	Differences between GEM and THGEM	36
4.4	The THGEM gain time-evolution.....	39
4.5	The hybrid photon detector prototype for COMPASS RICH-1 upgrade.....	42
4.6	Possible future direction of research	46
	Conclusion	48
	Bibliography	50
	List of Figures	52
	List of Abbreviations	54

Introduction

This thesis is devoted to the particle identification using Ring Cherenkov Detector Technology at COMPASS experiment at CERN was done at the Department of Low-Temperature Physics, Faculty of Mathematics and Physics of the Charles University in Prague in cooperation with CERN, Geneva, Switzerland.

COMPASS [1] is a physics experiment at the SPS – Super Proton Synchrotron accelerator complex. It is located at the European Organization for Nuclear Research in Geneva, Switzerland which is known under the abbreviation CERN [2] (derived from "Conseil Européen pour la Recherche Nucléaire").

The COMPASS experiment makes the use of the CERN SPS high-intensity secondary muon and hadron beams and polarized and unpolarized targets for the investigations of the nucleon spin structure and the spectroscopy of hadrons. Outgoing particles from the interactions of the beam particles with the targets are detected by a two-stage, large and small angle and momentum range spectrometers. Particle identification (PID) is achieved using hadron and electromagnetic calorimeters and in the first-stage of COMPASS large angle spectrometer also by Ring Imaging Cherenkov (RICH-1) counter.

COMPASS RICH-1 is a large fast gaseous Ring Imaging Cherenkov Detector, providing high quality hadron identification in the momentum range from 3 to 60 GeV/c. It has been successfully operated since 2002 with progressive optimization and long term mastering of the challenges from radiator gas (C_4F_{10}) purity, mirror alignment, photon detector performance, read-out system, heat control etc.

RICH counters for PID in the high momentum domain and in the large acceptance experiments like COMPASS require photon detectors covering extended surface (up to several square meters) to be able to accept Cherenkov photons in a wide angular range. When developing COMPASS RICH-1, an ideal approach was represented by gaseous photon detectors based on the multi wire proportional chambers (MWPC), which allow covering wide detection surface at affordable costs.

With the requirements to increase the muon and hadron beams intensity the Cherenkov photon detection in the central part of the COMPASS RICH-1 requires to cope with the counting rates of several $10^6/s$ per channel, and the trigger rates of up to 100 kHz. Therefore the central photon detector part based on MWPCs was replaced by multi-anode photomultiplier tubes (MAPMTs) coupled to individual fused silica lens telescopes, and fast read-out electronics based on MAD4 amplifier-discriminator and the dead-time free F1 TDC chip. The peripheral photon detection region is equipped with multi-wire proportional chambers with CsI photo-cathodes and the read-out system based on preamplifiers and flash ADC chips.

The novel and robust thick GEM-THGEM (Thick Gas Electron Multiplier) electron multiplier, coupled to a solid state photon converter is currently being developed to be used in the peripheral region to replace MWPC detection units used so far. This thesis project is a part of the efforts at COMPASS devoted to this important development for Cherenkov photon novel detection systems based on MicroMegas (Micro-Mesh Gaseous Structure) and GEM-THGEM for the peripheral RICH-1 photon detection region.

This master thesis is composed of Introduction, four chapters and Conclusion. After the Introduction, the first chapter brings the information about the COMPASS experiment in CERN, where the experimental part of this thesis was done. The second chapter is devoted to Cherenkov radiation – it's history, derivation of its properties and some applications, including Ring Imaging Cherenkov type of detectors for particle identification. The third chapter describes the RICH-1 detector as a part of the COMPASS arrangement. The fourth chapter is devoted to the current RICH-1 detector upgrade – the development of novel hybrid Cherenkov light detectors for the COMPASS RICH-1 based on the MicroMegas and the THGEM detectors and to the testing of the $300 \times 300 \text{ mm}^2$ prototype of such detector. In the Conclusion the main results of the thesis are summarized.

1 The COMPASS experiment in CERN

The COMPASS (Common Muon and Proton Apparatus for Structure and Spectroscopy) experiment aims to inspect hadron structure and dynamics in a length scale of about 10^{-15} m what is theoretically described by quantum chromodynamics (QCD). COMPASS in its current setup (Figures 1.1 and 1.2) is able to work with very high intensity beams, which reach values about 10^7 particles per second. Due to the presence of various detectors it is possible to detect both, the charged and the uncharged particles from beam-target interactions. The COMPASS setup allows inspecting different particles such as pions, kaons, protons and anti-protons using the beam tuning. We can schematically divide the COMPASS layout into several sections. The first section is composed by different targets used for each particular experiment, the Large Angle Spectrometer (LAS), the Small Angle Spectrometer (SAS), the Trigger, the Central Data Recording (CDR), the Data Collection and Acquisition (DAQ) Systems. In the LAS and SAS spectrometers the powerful tracking systems including about 350 planes, particle identification systems including muon walls (MW), electromagnetic (ECAL) and hadron (HCAL) calorimeters and magnetic spectrometers with magnetic dipole magnets are used. As the part of the PID system in LAS the unique large fast gaseous Ring Imaging Cherenkov Detector – RICH-1 is used.

As already mentioned, the COMPASS experiment is connected to SPS accelerator, which offers different kinds of particles in the beam for COMPASS starting with the secondary hadron beams (proton, kaon pion) and tertiary negatively and positively charged muons and ending with electrons. The change between different types of the beam takes approximately half an hour. The beam enters the target which can be surrounded by different scintillation detectors. Material of the target can be varied, the most commonly used are unique polarized proton (NH_3) and deuteron (${}^6\text{LiD}$) solid state targets, unpolarized liquid hydrogen and different solid state targets.

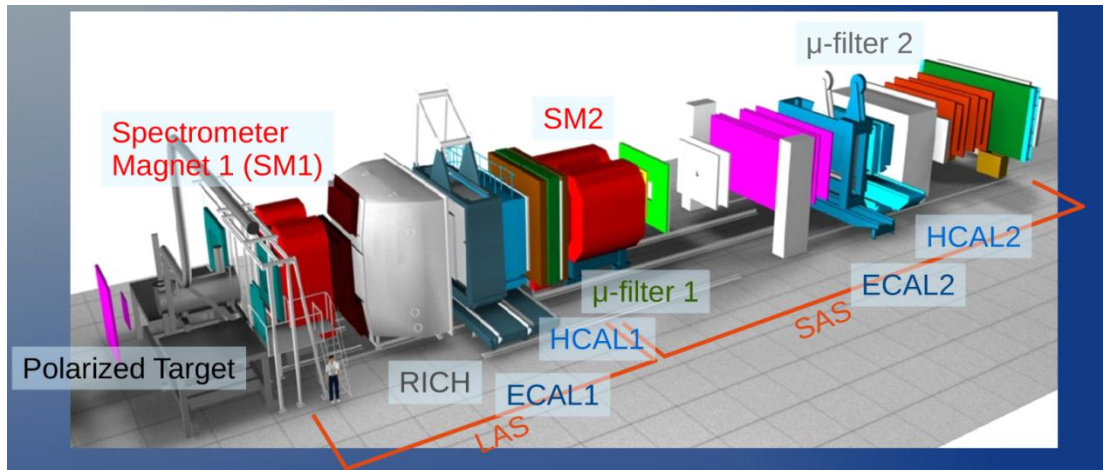


Figure 1.1: COMPASS setup in 2014 [3].

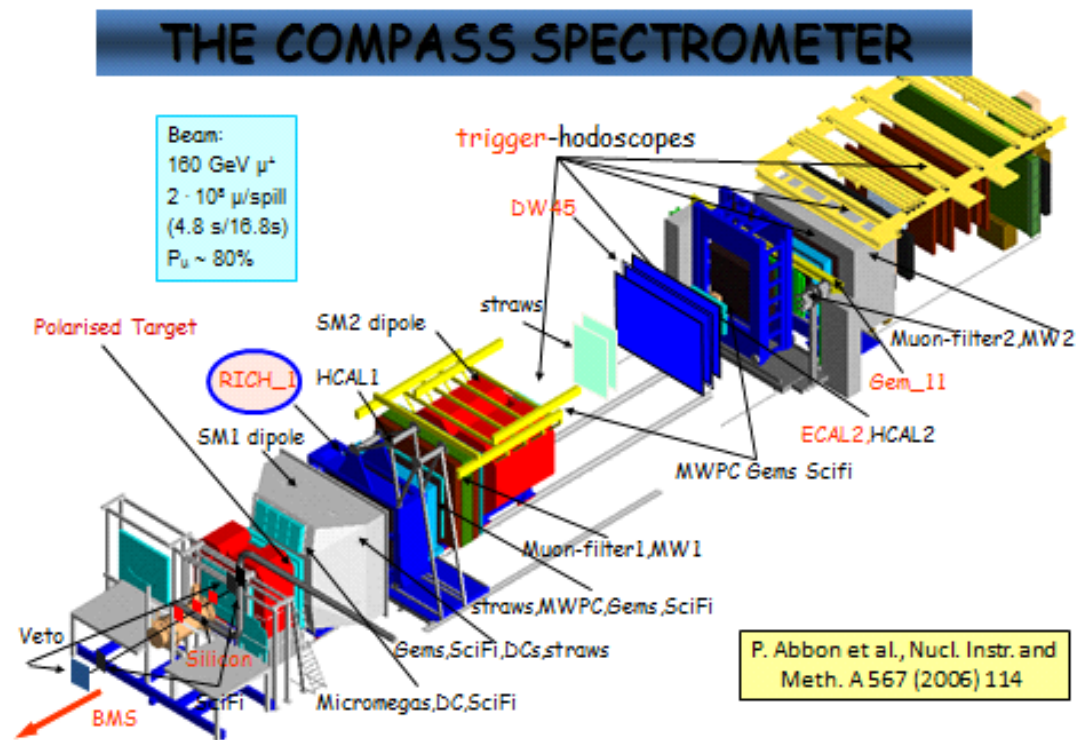


Figure 1.2: COMPASS setup.

2 Cherenkov radiation

2.1 Description

Cherenkov radiation is composed of photons which are emitted when a charged particle comes through a matter environment. If the speed of the particle is greater than the speed of light in particular matter environment, the emitted light interferes and creates a light cone. You can imagine this on an example of a duck floating on the water. If it moves faster than stir spreads in the water, you can see a furrow behind of it. Another example in three dimensions could be a supersonic aircraft which leaves behind a shock wave in a shape of a cone, where it is possible to hear aircraft noise. Cherenkov particle creates a similar cone behind it, which consists of light.

Less popular explanation is that Cherenkov particle polarizes particles along its trajectory and they emit photons by depolarization. In fact, surrounding molecules are excited by the Cherenkov particle and they emit photons, when they go back to the basic energetic level [4]. We can also perceive these photons as an electromagnetic wave. In the appropriate angle, we can observe the constructive wave interference and see the light cone.

2.2 Historical progress

An English scientist Oliver Heaviside was at the birth of theory, which predicts Cherenkov radiation [5]. This remarkable man made an extensive research in electromagnetic area despite he was an autodidact. The uniqueness of this man is reflected by the following quote by Govorkov, connected to the discovery of Cherenkov radiation: “A genius, Heaviside was half a century in advance of his time in his calculations and predictions, but unfortunately he was not understood by his contemporaries. His works were forgotten, and scientists had to start from the beginning, this time from experiment.”

For the first time, Cherenkov radiation was observed by Maria Curie-Skłodowska and Pierre Currie. During an experiment that aimed to separate radium, they observed a blue radiation, but they paid no attention to it.

The scientist, who explained this phenomenon and who the radiation was named after was Pavel Alexejevich Cherenkov. In 1958 Pavel Cherenkov together with Ilya Frank and Igor Tamm were awarded a Nobel Prize in Physics. Ilya M. Frank and Igor J. Tamm explained Cherenkov radiation on a basis of Maxwell's equations [6].

2.3 Derivations

We will show three different derivations of properties of Cherenkov radiation. In the first derivation, we will use only the classical physic. The second derivation uses electrodynamics similar to Frank – Tamm derivation. The third derivation is solved from the perspective of quantum mechanics.

2.3.1 Classical derivation

In this part we will think about what classical physic, especially geometrical optic, can show about Cherenkov radiation.

In section 2.1 we got to know that charged particle passing through the matter environment emits light and this light interferes. Now we will show that the interference condition is that the speed of Cherenkov particle is greater or equal than the speed of light in this environment. We will mark these variables:

v – speed of the Cherenkov particle,

c – speed of light in vacuum,

n – refractive index,

c' – speed of light in the given matter environment.

For size of c' apply the formula:

$$c' = \frac{c}{n} \quad (1)$$

In the following picture (Figure 2.1) you can see several equiphase surfaces that belong to Cherenkov particle for case $c' > v$. It is visible that equiphase surfaces don't cross, therefore interference can't occur.

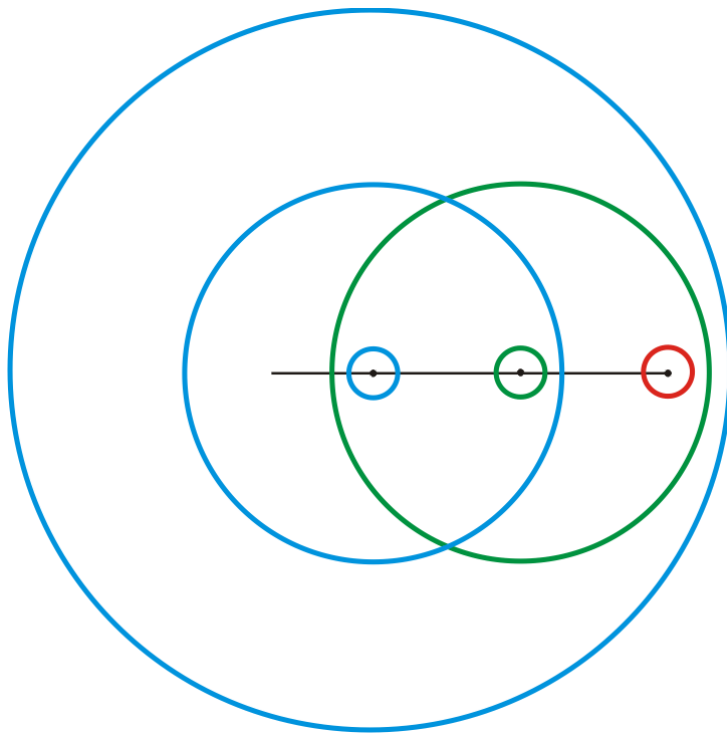


Figure 2.1: Spreading wave scheme A.

In the next picture (Figure 2.2), there are equiphase surfaces for condition $c' < v$. Two black lines sign places, where constructive interference appears.

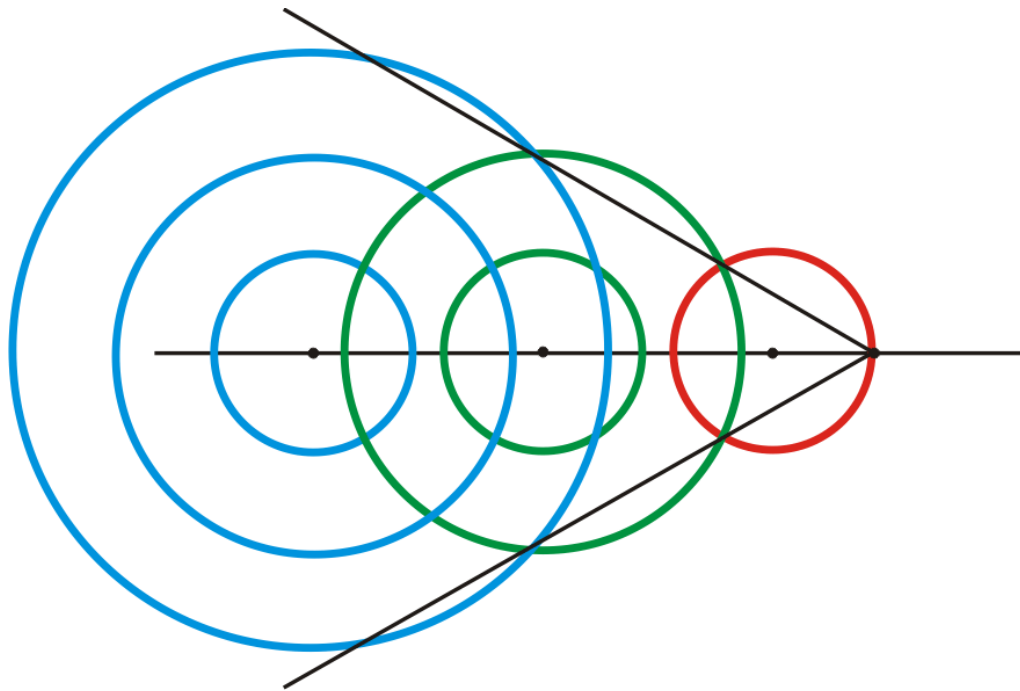


Figure 2.2: Spreading wave scheme B.

For completeness the last picture (Figure 2.3) shows equiphase surfaces of one Cherenkov particle for case $c' = v$.

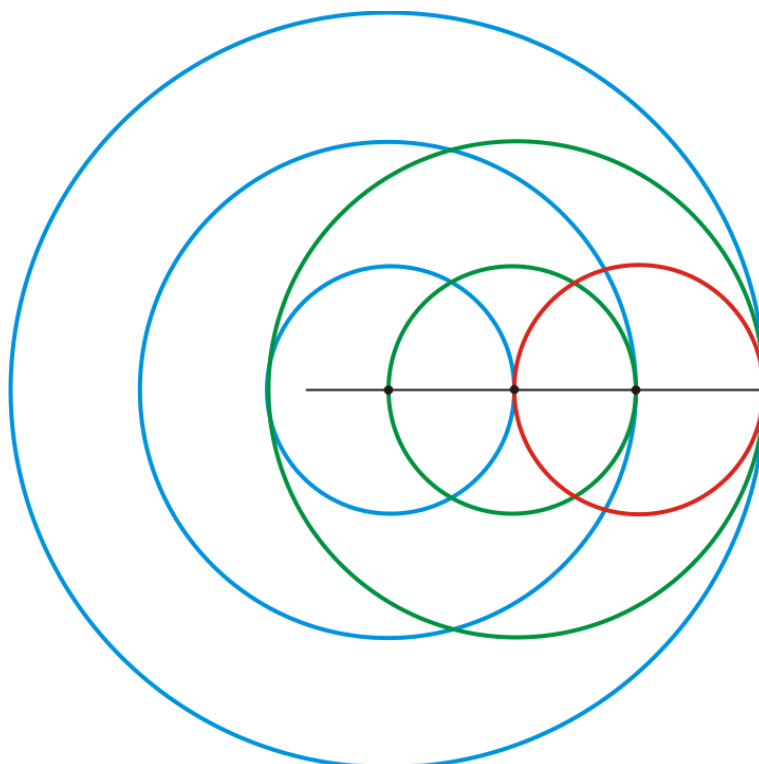


Figure 2.3: Spreading wave scheme C.

Now we consider case $c' < v$. Due to symmetry two black lines in (Figure 2.2) represent a cone in space. Let's express cosine of angle θ which describes direction of propagation of the Cherenkov light.

Cherenkov particle moves with velocity v , during the time t it will cover a distance s_c . We can write:

$$s_c = vt, \quad (2)$$

similarly, the light moves by velocity c' , during the same time t it will cover a distance s_p . The relation is:

$$s_p = c't. \quad (3)$$

For expression of cosine of angle θ we will draw the following picture (Figure 2.4):

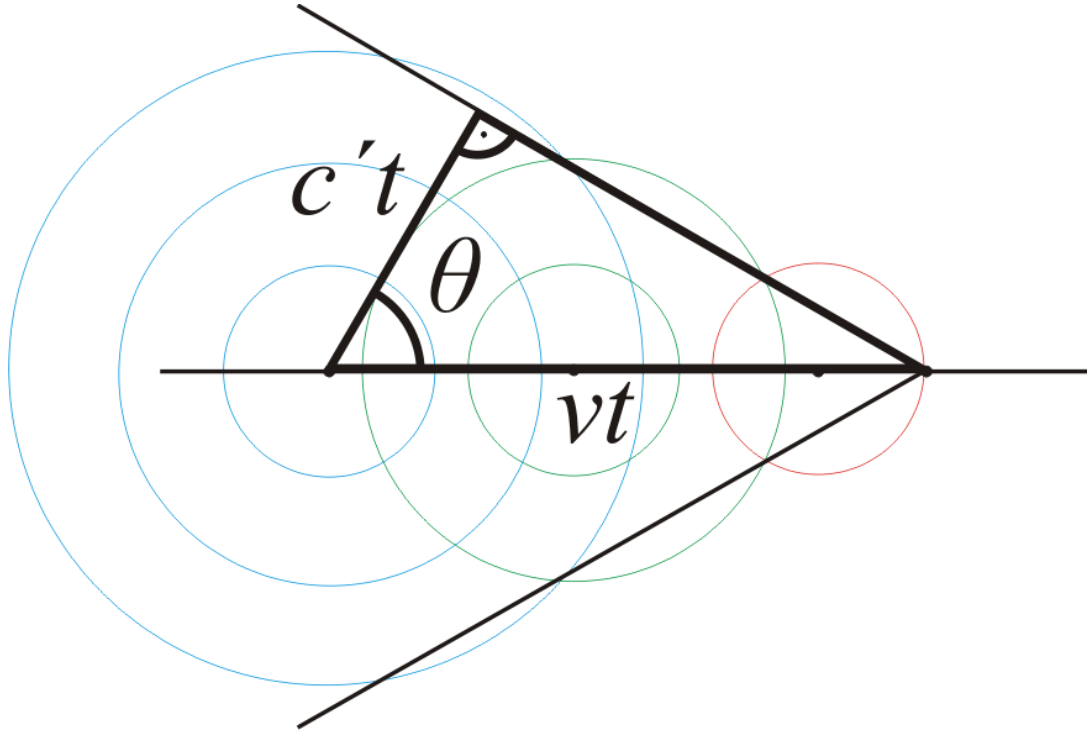


Figure 2.4: Angle of interference scheme.

Hence

$$\cos \theta = \frac{c't}{vt} = \frac{c'}{v}. \quad (4)$$

For obvious reasons we consider angle θ in interval $\theta \in \left(0; \frac{\pi}{2}\right)$.

It is visible that with increasing velocity of particle v , $\cos \theta$ and the angle θ are getting larger. This means that the vertex angle of a cone is getting smaller. It means that for bigger velocity the light cone is thinner. We can compare it to the example from section 2.1. If the duck is moving faster, the furrow would be thinner. For supersonic aircraft the effect is the same.

2.3.2 Electrodynamics derivation

In the following text we will show a part of derivation which leads to Frank-Tamm formula. I. J. Tamm and J. M. Frank used classical electrodynamics as an instrument – as well we are doing.

We will start with Maxwell equations:

$$\nabla \cdot \mathbf{D} = \rho, \quad (5)$$

$$\nabla \cdot \mathbf{B} = 0, \quad (6)$$

$$\nabla \times \mathbf{E} = -\frac{\partial \mathbf{B}}{\partial t}, \quad (7)$$

$$\nabla \times \mathbf{H} = \frac{\partial \mathbf{D}}{\partial t} + \mathbf{j}. \quad (8)$$

Where the following variables mean:

\mathbf{E} – electric field,

\mathbf{D} - electric displacement field,

\mathbf{B} – magnetic field,

\mathbf{H} – magnetic H-field,

ε – permittivity,

μ – permeability,

ρ – electric charge density,

\mathbf{j} – electric current density.

Relations between \mathbf{E} and \mathbf{D} and relation between \mathbf{B} and \mathbf{H} are:

$$\mathbf{D} = \epsilon \mathbf{E} = \epsilon_0 \epsilon_r \mathbf{E}, \quad (9)$$

$$\mathbf{B} = \mu \mathbf{H} = \mu_0 \mu_r \mathbf{H}. \quad (10)$$

Where ϵ_0 and μ_0 are permittivity and permeability of vacuum and ϵ_r and μ_r are relative permittivity and relative permeability.

We used ϵ and μ as constants. In some environments ϵ and μ can be tensors of the second grade.

Let us consider Maxwell's equations in vacuum, where charge density $\rho = 0$ as well as electric current density $\mathbf{j} = \mathbf{0}$. We apply to equation (7) an operator curl:

$$\nabla \times (\nabla \times \mathbf{E}) = -\nabla \times \frac{\partial \mathbf{B}}{\partial t}. \quad (11)$$

We modify equation using well known identity $\nabla \times (\nabla \times \mathbf{A}) = \nabla(\nabla \cdot \mathbf{A}) - (\nabla \cdot \nabla) \mathbf{A}$ and switch operator curl and partial derivation on the right side.

$$\nabla(\nabla \cdot \mathbf{E}) - \Delta \mathbf{E} = -\frac{\partial \nabla \times \mathbf{B}}{\partial t}. \quad (12)$$

From equation (5) in vacuum we can clear the result $\nabla \cdot \mathbf{E} = 0$. Using (10) we can rewrite the equation to:

$$\Delta \mathbf{E} - \mu_0 \frac{\partial \nabla \times \mathbf{H}}{\partial t} = \mathbf{0}. \quad (13)$$

Appointing from equation (8) and considering relation (9) we can write:

$$\Delta \mathbf{E} - \epsilon_0 \mu_0 \frac{\partial^2 \mathbf{E}}{\partial t^2} = \mathbf{0}. \quad (14)$$

This is a wave equation. We have found that electric component of an electromagnetic field spreads like a wave.

Let us sign:

$$\epsilon_0 \mu_0 = \frac{1}{c^2}. \quad (15)$$

Constant c means speed of the wave spreading. In this case it is the speed of light.

Look at equation 6. From this equation it is obvious that for \mathbf{B} we can write:

$$\mathbf{B} = \nabla \times \mathbf{A}, \quad (16)$$

where the a variable named \mathbf{A} is the vector potential. Let us focus on equation (7) and replace \mathbf{B} from the previous equation.

$$\nabla \times \mathbf{E} + \frac{\partial}{\partial t} (\nabla \times \mathbf{A}) = \mathbf{0}, \quad (17)$$

$$\nabla \times \left(\mathbf{E} + \frac{\partial \mathbf{A}}{\partial t} \right) = \mathbf{0}. \quad (18)$$

Hence this is the relation between \mathbf{E} and scalar electromagnetic potential φ :

$$\mathbf{E} + \frac{\partial \mathbf{A}}{\partial t} = -\nabla \varphi, \quad (19)$$

$$\mathbf{E} = -\nabla \varphi - \frac{\partial \mathbf{A}}{\partial t}. \quad (20)$$

In the following lines we will try to find the wave equation for potentials \mathbf{A} and φ . We will start with equation (8). After multiplication μ and using relations (9) and (10) we get:

$$\nabla \times \mu \mathbf{H} - \epsilon \mu \frac{\partial \mathbf{E}}{\partial t} = \mu \mathbf{j} \quad (21)$$

To modify the equation we use relations (16) and (20).

$$\nabla \times (\nabla \times \mathbf{A}) - \varepsilon\mu \frac{\partial}{\partial t} \left(-\nabla\varphi - \frac{\partial \mathbf{A}}{\partial t} \right) = \mu \mathbf{j}, \quad (22)$$

$$\Delta \mathbf{A} - \nabla(\nabla \cdot \mathbf{A}) - \varepsilon\mu \left(\frac{\partial \nabla\varphi}{\partial t} + \frac{\partial^2 \mathbf{A}}{\partial t^2} \right) = -\mu \mathbf{j}, \quad (23)$$

$$\Delta \mathbf{A} - \varepsilon\mu \frac{\partial^2 \mathbf{A}}{\partial t^2} - \nabla \left(\nabla \cdot \mathbf{A} + \varepsilon\mu \frac{\partial \varphi}{\partial t} \right) = -\mu \mathbf{j}. \quad (24)$$

Gradient in the last equation is not given unequivocal. We can require the expression in parenthesis to be equal to zero:

$$\nabla \cdot \mathbf{A} + \varepsilon\mu \frac{\partial \varphi}{\partial t} = 0. \quad (25)$$

The last condition is often called Lorenz gauge condition. By using of Lorenz gauge condition we get:

$$\Delta \mathbf{A} - \varepsilon\mu \frac{\partial^2 \mathbf{A}}{\partial t^2} = -\mu \mathbf{j}. \quad (26)$$

It is the wave equation for vector potential \mathbf{A} , which we were looking for. We can sign:

$$\varepsilon\mu = \frac{1}{c'^2} = \frac{n^2}{c^2}, \quad (27)$$

where c' is the speed of the spreading wave in the particular material environment and n is the refractive index.

We have to find the wave equation for φ . For this purpose we take the expression of \mathbf{E} , equation (20), and we apply divergence on it.

$$\nabla \cdot \mathbf{E} = -\nabla \cdot \nabla\varphi - \nabla \cdot \left(\frac{\partial \mathbf{A}}{\partial t} \right). \quad (28)$$

In the next step we use equation (5) and then, from the Lorentz gauge condition (25), we express the expression $\nabla \cdot \mathbf{A}$.

$$\frac{\rho}{\varepsilon} = -\nabla \cdot \nabla \varphi - \frac{\partial}{\partial t}(\nabla \cdot \mathbf{A}). \quad (29)$$

$$\Delta \varphi - \varepsilon \mu \frac{\partial^2 \varphi}{\partial t^2} = -\frac{\rho}{\varepsilon}. \quad (30)$$

We have found the wave equation for φ . Now, we can rewrite equations (26) and (30) using relation (27).

$$\Delta \mathbf{A} - \frac{n^2}{c^2} \frac{\partial^2 \mathbf{A}}{\partial t^2} = -\mu \mathbf{j}, \quad (31)$$

$$\Delta \varphi - \frac{n^2}{c^2} \frac{\partial^2 \varphi}{\partial t^2} = -\frac{\rho}{\varepsilon}. \quad (32)$$

We have obtained wave-equations for vector potential and scalar electromagnetic potential that are created by electric current density \mathbf{j} and by electric charge density ρ . We will consider that the Cherenkov particle is an electron, which is a point-particle. We can express the electric charge density ρ_c of a non-moving electron as:

$$\rho_c = e\delta(\mathbf{r}), \quad (33)$$

where e means elementary charge and $\delta(\mathbf{r})$ means Dirac's delta-function in the place defined by the position of vector \mathbf{r} .

Electric charge density ρ for a constantly moving particle with a velocity \mathbf{v} in time t is:

$$\rho = e\delta(\mathbf{r} - \mathbf{v}t). \quad (34)$$

Similarly we express the electric current density \mathbf{j} as:

$$\mathbf{j} = e\mathbf{v}\delta(\mathbf{r} - \mathbf{v}t). \quad (35)$$

By the substitution into the equation (31) and (32) we obtain:

$$\Delta \mathbf{A} - \frac{n^2}{c^2} \frac{\partial^2 \mathbf{A}}{\partial t^2} = -\mu e \mathbf{v} \delta(\mathbf{r} - \mathbf{v}t), \quad (36)$$

$$\Delta \varphi - \frac{n^2}{c^2} \frac{\partial^2 \varphi}{\partial t^2} = -\frac{e \delta(\mathbf{r} - \mathbf{v}t)}{\varepsilon}. \quad (37)$$

We are interested in conditions, where the solution of equations (36) and (37) has the form of a plane wave. The standard expression for a plane wave is:

$$\varphi = C \cdot e^{i\mathbf{k} \cdot (\mathbf{r} - \mathbf{v}t)}, \quad (38)$$

where C is a constant and \mathbf{k} is a wave vector.

Let's look at the exponent in equation (38):

$$\begin{aligned} i\mathbf{k} \cdot (\mathbf{r} - \mathbf{v}t) &= i(k_x, k_y, k_z) \cdot [(x, y, z) - (v_x, v_y, v_z)] = \\ &= ik_x(x - v_x t) + ik_y(y - v_y t) + ik_z(z - v_z t). \end{aligned} \quad (39)$$

The indexed variables are the vector components in Cartesian coordinates. Hence, we can calculate the Laplace operator:

$$\Delta \varphi = (-k_x^2 - k_y^2 - k_z^2) C \cdot e^{i\mathbf{k} \cdot (\mathbf{r} - \mathbf{v}t)}. \quad (40)$$

For squared wave vector let's apply:

$$\mathbf{k}^2 = k_x^2 + k_y^2 + k_z^2, \quad (41)$$

hence we can write:

$$\Delta \varphi = -\mathbf{k}^2 C \cdot e^{i\mathbf{k} \cdot (\mathbf{r} - \mathbf{v}t)}. \quad (42)$$

Let's look at the next part of equation (37) which contains second partial derivation by time. For the first partial derivation let's apply:

$$\begin{aligned}\frac{\partial \varphi}{\partial t} &= -ik_x v_x C \cdot e^{i\mathbf{k} \cdot (\mathbf{r} - \mathbf{v}t)} - ik_y v_y C \cdot e^{i\mathbf{k} \cdot (\mathbf{r} - \mathbf{v}t)} - ik_z v_z C \cdot e^{i\mathbf{k} \cdot (\mathbf{r} - \mathbf{v}t)} = \\ &= -i(\mathbf{k} \cdot \mathbf{v})C \cdot e^{i\mathbf{k} \cdot (\mathbf{r} - \mathbf{v}t)}.\end{aligned}\quad (43)$$

Hence for the second partial derivation:

$$\frac{\partial^2 \varphi}{\partial t^2} = i^2 (\mathbf{k} \cdot \mathbf{v})^2 C \cdot e^{i\mathbf{k} \cdot (\mathbf{r} - \mathbf{v}t)} = -(\mathbf{k} \cdot \mathbf{v})^2 C \cdot e^{i\mathbf{k} \cdot (\mathbf{r} - \mathbf{v}t)}.\quad (44)$$

On the right side of equation (37) is Dirac's delta function, which is equal to zero everywhere, except places, where the Cherenkov particle is localized, namely in $\mathbf{r} = \mathbf{v}t$. We will not consider these places.

We can substitute equations (42) and (44) into equation (37):

$$-\mathbf{k}^2 C \cdot e^{i\mathbf{k} \cdot (\mathbf{r} - \mathbf{v}t)} + \frac{n^2}{c^2} (\mathbf{k} \cdot \mathbf{v})^2 C \cdot e^{i\mathbf{k} \cdot (\mathbf{r} - \mathbf{v}t)} = 0\quad (45)$$

After fraction by $C \cdot e^{i\mathbf{k} \cdot (\mathbf{r} - \mathbf{v}t)}$ and modification we get this condition:

$$k^2 - \frac{n^2}{c^2} (\mathbf{k} \cdot \mathbf{v})^2 = 0.\quad (46)$$

In the last equation the dot product is present. It has the meaning of circular frequency:

$$\omega = \mathbf{k} \cdot \mathbf{v}.\quad (47)$$

It expresses that the circular frequency ω depends on the direction of the wave spreading and on the direction of velocity \mathbf{v} of the Cherenkov particle. We denote the angle between \mathbf{k} and \mathbf{v} as θ and we can write:

$$\omega = \mathbf{k} \cdot \mathbf{v} = kv \cos \theta\quad (48)$$

After substitution into condition (46) we get:

$$k^2 - \frac{n^2}{c^2} (kv \cos \theta)^2 = 0\quad (49)$$

We will express the cosine of angle θ :

$$\cos \theta = \frac{c}{\bar{n}v} = \frac{c'}{v}. \quad (50)$$

This condition can be satisfied only if:

$$c' \leq v. \quad (51)$$

It means that the Cherenkov particle has to move faster than the speed of light in the given matter environment [7],[8].

2.3.3 Quantum mechanics derivation

At the beginning of deriving Cherenkov radiation properties, we have to realize, that we consider microscopic particles which are moving very fast. We can compare the speed of these particles to the speed of light. For this reason we can't think of these particles in a classical way, but we have to use relativistic expressions.

In the following lines we will use conservation of momentum to obtain dependence of angle θ which is determined by the direction of the particle's propagation and the wave propagation (electromagnetic wave which corresponds to the emitted light).

We will mark these variables:

P – momentum of incoming particle,

P_e – momentum of particle after emitting photon,

P_p – momentum of Cherenkov photon.

The conservation of momentum tells:

$$P_e = P - P_p. \quad (52)$$

For squared sizes of these vectors we apply:

$$P_e^2 = P^2 + P_p^2 - 2\mathbf{P} \cdot \mathbf{P}_p. \quad (53)$$

Momentum of a photon is:

$$\mathbf{P}_p = h\mathbf{k}, \quad (54)$$

where h is the Planck constant and \mathbf{k} is a wave vector, heading to the direction of propagation of the photon.

Considering the law of conservation of energy we obtain:

$$\sqrt{P_e^2 c^2 + m_0^2 c^4} = \sqrt{P^2 c^2 + m_0^2 c^4} - hv. \quad (55)$$

The variable m_0 is the rest mass of the Cherenkov particle and ν is the photon's frequency.

In the next step we divide the equation by the speed of light c and substitute P_e^2 from equation (53):

$$\sqrt{P^2 + h^2 k^2 - 2h\mathbf{P} \cdot \mathbf{k} + m_0^2 c^2} = \sqrt{P^2 + m_0^2 c^2} - \frac{h\nu}{c}. \quad (56)$$

Then we square the equation:

$$P^2 + h^2 k^2 - 2h\mathbf{P} \cdot \mathbf{k} + m_0^2 c^2 = P^2 + m_0^2 c^2 + \frac{h^2 \nu^2}{c^2} - 2\frac{h\nu}{c} \sqrt{P^2 + m_0^2 c^2} \quad (57)$$

$$h^2 k^2 - 2h\mathbf{P} \cdot \mathbf{k} = \frac{h^2 \nu^2}{c^2} - 2\frac{h\nu}{c} \sqrt{P^2 + m_0^2 c^2}. \quad (58)$$

We use relation for scalar multiplication:

$$\mathbf{P} \cdot \mathbf{k} = pk \cos \theta. \quad (59)$$

Dependence of angle θ is exactly what we want to express. It is determined by the direction of the particle's propagation and the direction of the wave propagation.

We will substitute for scalar multiplication $\mathbf{P} \cdot \mathbf{k}$ in equation (58) from (59) and express $\cos \theta$.

$$h^2 k^2 - 2hPk \cos \theta = \frac{h^2 v^2}{c^2} - 2 \frac{hv}{c} \sqrt{P^2 + m_0^2 c^2}, \quad (60)$$

$$\cos \theta = \frac{hk}{2P} - \frac{hv^2}{2kPc^2} + \frac{v}{kPc} \sqrt{P^2 + m_0^2 c^2}, \quad (61)$$

$$\cos \theta = \frac{hk}{2P} - \frac{hv^2}{2kPc^2} + \frac{v}{kc} \sqrt{1 + \frac{m_0^2 c^2}{P^2}}. \quad (62)$$

Cherenkov particle moves very fast. Because of this fact we have to use relativistic expression of momentum \mathbf{P} .

$$\mathbf{P} = \frac{m_0 v}{\sqrt{1 - \frac{v^2}{c^2}}}, \quad (63)$$

where v means velocity of the Cherenkov particle.

Let us solve the square root from equation (62):

$$\sqrt{1 + \frac{m_0^2 c^2}{P^2}} = \sqrt{1 + \frac{m_0^2 c^2}{\frac{m_0^2 v^2}{1 - \frac{v^2}{c^2}}}} = \sqrt{1 + \frac{c^2}{\frac{c^2 v^2}{c^2 - v^2}}} = \sqrt{1 + \frac{c^2 - v^2}{v^2}} = \frac{c}{v}. \quad (64)$$

By using this relation in equation (62) we finally get this equation:

$$\cos \theta = \frac{hk}{2P} \left(1 - \frac{v^2}{k^2 c^2}\right) + \frac{v}{kv}. \quad (65)$$

In a material environment with refractive index n we can write relations:

$$c' = \frac{c}{n}, \quad (66)$$

$$v = c'k = \frac{c'}{\lambda}, \quad (67)$$

where λ is wavelength.

We modify equation (65) by using previous relations:

$$\cos \theta = \frac{hk}{2P} \left(1 - \frac{1}{n^2} \right) + \frac{c'}{v}. \quad (68)$$

It is visible that we gain reasonable results only if we assume $c' < v$. Therefore particle which makes uniform rectilinear motion slower than the speed of light in a material environment can't emit a photon.

We can see that for $h \rightarrow 0$ equation (68) is reduced to equation (4), which was obtained by classical physic [7].

2.4 Some applications

We can use Cherenkov radiation to inspect some features of the particles creating Cherenkov light. If we measure the direction of the cone axis, we know which positions the observed particle passed through the medium. If we know the central angle (Cherenkov angle) of the Cherenkov light cone we can learn something about the particle momentum and of course about the related energy. On the other hand, having the possibility to measure independently the momentum (or the energy) of the particles producing Cherenkov light in the medium with refractive index “ n ” and measuring the Cherenkov angle we can identify the mass of the particle creating the Cherenkov light. Ring Imaging Cherenkov Detectors (RICH) are based on this principle for particle identification. This type of detectors is now broadly used in many particle and astroparticle physics experiments. This type of detector is an important part of the particle identification system in the COMPASS experiment.

2.5 Ring Imaging Cherenkov detectors

2.5.1. Cherenkov light imaging – basic formulas

As it was deduced in the section 2.3, emission of Cherenkov light is created only when the Cherenkov particle is faster than the speed of light in the medium. Hence the minimal particle's velocity v_{\min} , during which the radiation is produced, is equal to c' .

We can consider a threshold β :

$$\beta = \frac{v}{c}. \quad (69)$$

The minimal value of β is for $v = v_{\min}$:

$$\beta_{\min} = \frac{v_{\min}}{c} = \frac{c'}{c} = \frac{1}{n}. \quad (70)$$

We can express the angle of emission which was introduced for instance in equation (4) by using threshold β like:

$$\cos \theta = \frac{c'}{v} = \frac{c'}{\beta c} = \frac{1}{\beta n}. \quad (71)$$

We can see that for $\beta = \beta_{\min}$ the following expression is valid:

$$\cos \theta = \frac{1}{\beta_{\min} n} = \frac{n}{n} = 1, \quad (72)$$

hence the angle θ is equal to zero, which means that the direction of propagation of Cherenkov light is identical with the propagation of Cherenkov particle.

The following extreme case is for an ultra-relativistic particle which travels at nearly the speed of light. This case corresponds to the value of threshold β approaching one. For cosine of the angle θ let's apply:

$$\cos \theta = \frac{1}{\beta n} = \frac{1}{n}. \quad (73)$$

Number of emitted photons N related to the element of distance x and the element of wavelengths λ is given by this relation:

$$\frac{\partial N^2}{\partial x \partial \lambda} = \frac{2\pi\alpha Z^2}{\lambda^2} \sin^2 \theta, \quad (74)$$

where:

λ – fine structure constant,

Z – number of elemental charges.

2.5.2. Ring Imaging Cherenkov detector – the basis

Cherenkov photons, which are produced in the radiator are reflected from the spherical mirrors with radius of curvature R . For the focal length F , we apply the well known relation:

$$F = \frac{R}{2}. \quad (75)$$

In RICH-1 experimental arrangement the focal length F is equal to the radiator length L .

Radius of the ring on the focal surface r is related with the mentioned optical parameters through the relation:

$$r = F \tan \theta = \frac{R}{2} \tan \theta. \quad (76)$$

In a small angle approximation we can write:

$$r = \frac{R}{2} \sqrt{2 - \frac{2}{n} \sqrt{1 + \frac{m^2 p^2}{c^2}}}, \quad (77)$$

where:

m – mass of the Cherenkov particle

p – momentum of the Cherenkov particle

When the momentum of the particle creating Cherenkov light is measured for instance by a magnetic spectrometer, the measured radius of the ring, equation (77), allows the determination of the mass of the Cherenkov particle, e.i. to identify the particle.

3 COMPASS RICH-1

3.1 Experimental arrangement

The Ring Imaging Cherenkov (RICH) detector is used for the identification of charged particles as pions, kaons and protons with momenta between 1 GeV/c to 50 GeV/c. It is based on the Cherenkov effect i.e. emission of electromagnetic radiation when charged particle is passing through a dielectric medium with velocity greater than the phase velocity of light in that medium. COMPASS RICH-1 detector is located in LAS (Large Angle Spectrometer) area and it operates in angles $250 \text{ mrad} \times 150 \text{ mrad}$ (horizontal \times vertical).

The RICH-1 detector is composed of three parts (see Figures 3.1 and 3.2): gas vessel, focusing optics and detection system.

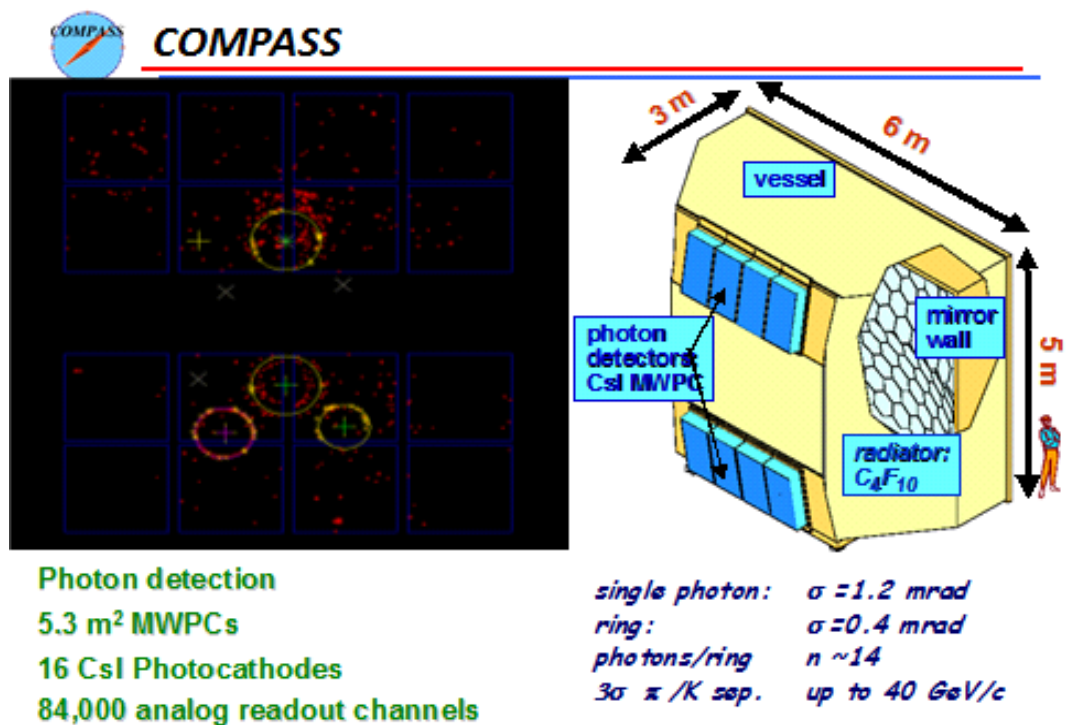


Figure 3.1: COMPASS RICH-1 detector [9].

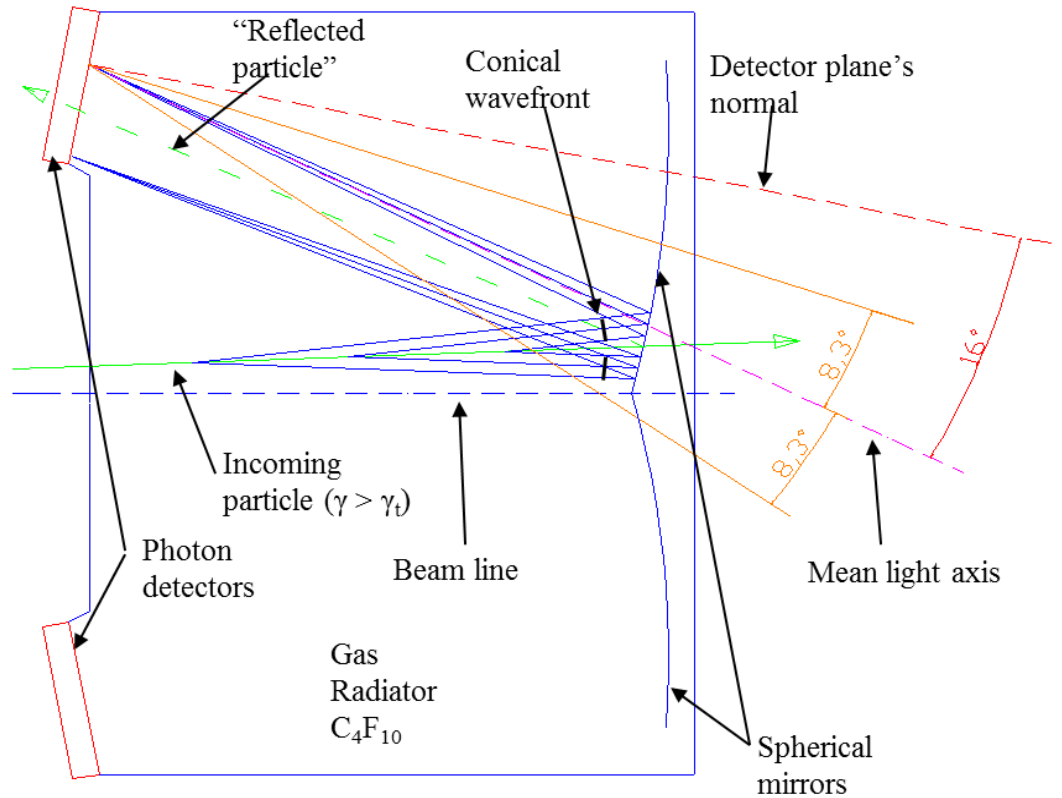


Figure 3.2: COMPASS RICH-1 detector – schematic view [9].

3.1.1 Gas vessel

The gas vessel is 3 meters long and it has the volume of about 80 m^3 . The vessel is filled with C_4F_{10} gas at a pressure of 1 Pa as the active medium – radiator environment which the Cherenkov particle passes through and where the fast particle produces the Cherenkov radiation.

The gas C_4F_{10} was chosen as a radiator due to its properties, especially its refractive index. It ensures good transparency of the medium for Cherenkov light with ultra violet wave length higher than 160 nm. To ensure good and stable transparency level it is essential to purify the gas regularly.

The refractive index of C_4F_{10} gas corresponds to Cherenkov threshold 3 GeV/c for pions, 9 GeV/c for kaons and 17 GeV/c for protons.

3.1.2 Focusing optics

Cherenkov photons produced in the gas vessel are reflected with two sets of mirrors. The mirror reflective part consists of two mosaical spherical mirror walls consisting of 116 hexagonal and pentagonal mirrors of total surface of 21m². As the Cherenkov photons are usually in the ultraviolet range, the mirrors must be made very precisely and must be able to reflect the light in this wavelength range with high efficiency. You can see the range of momenta for the identification of different particles with COMPASS RICH-1 detector in Figure 3.3. It is worth mentioning that the Czech Republic left an appreciable mark on the optical device inasmuch as the mirrors were made in the IMMA Turnov company – Figure 3.4.

3.1.3 Detection system

The detection plate is separated into 16 parts which are divided into two groups – into the lower and upper detector – as shown in the Figures 3.4 and 3.5.

The photo detection is currently based mainly on MWPC detectors equipped with CsI photocathodes. The Cherenkov light is converted by the photocathode and the produced photoelectrons are amplified by the MWPC. The central part of the Cherenkov photon detection system is equipped with fast multi-anode photomultipliers. There is currently an extensive R&D ongoing to produce relatively cheap (with respect to photomultipliers) and much superior detectors based on THGEM technology (i.e. GEM where the thin isolating layer is replaced by a more robust printed circuit board) to replace the rest of the system.

particle identification with Compass RICH

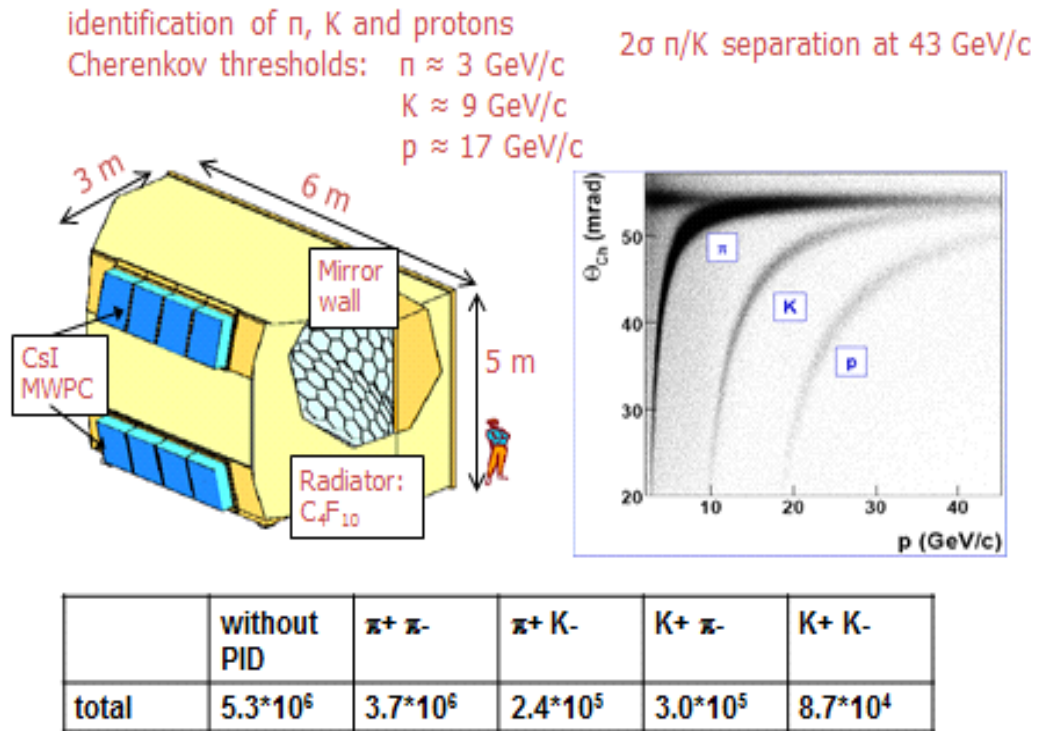


Figure 3.3: Particle identification with COMPASS RICH-1 [9].

3.2 Detector upgrade

At the beginning the detection surface of RICH-1 consisted of MWPC – multi-wire proportional chambers (MWPC). The gain wasn't higher than 5×10^4 ; high level of background was present especially in the area around the beam and the dead time was about 3.5 μs . In the first upgrade of the photon detection system the front-end electronics of MWPC were replaced. As the result the dead time was reduced to values between 400 ns and 3 μs and the related losses of the data were reduced to nearly 5%. Moreover the new electronics uses triple sampling which upgrades time resolution. The ratio between signal and background was also increased from 0.35 up to 2.13. So far the multi-wire proportional chambers were retained in their positions in three quarters of the detection surface. This solution was chosen in an effort to reduce costs.

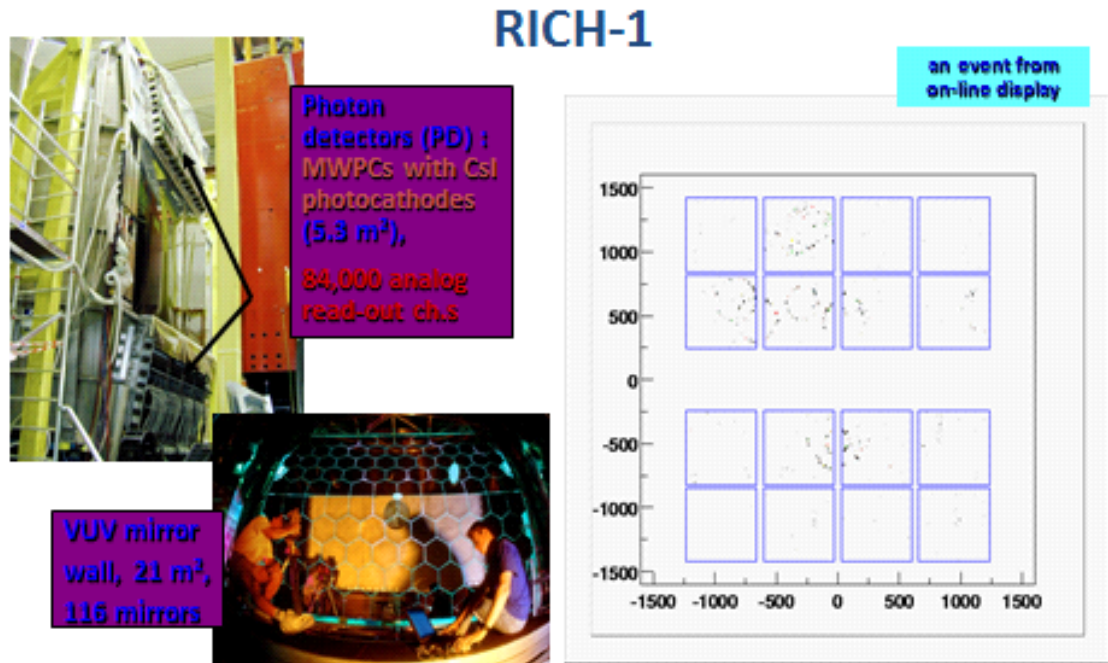


Figure 3.4: COMPASS RICH-1 detector – mirror system and photon detection [9].

For the four inner photon detection sections the MWPCs were replaced by multi-anode (sixteen channels) photomultiplier Hamamatsu tubes (MAPMT) sensitive also to ultraviolet photon wavelength region. Because of the need to increase the effective detection area each MAPMT is coupled to an optical telescope (see Figures 3.6 and 3.7).

The detection system which uses MAPMTs is able to detect approximately four times more photons than the previous MWPC system, so the ring may consist of about 60 photons. The time resolution of MAPMTs is under 1 ns. Another

MAPMT's advantage is that it is able to work in a wider wavelength range. You can see the comparison between MAPMT and MWPC in the Figures 3.8 and 3.9.

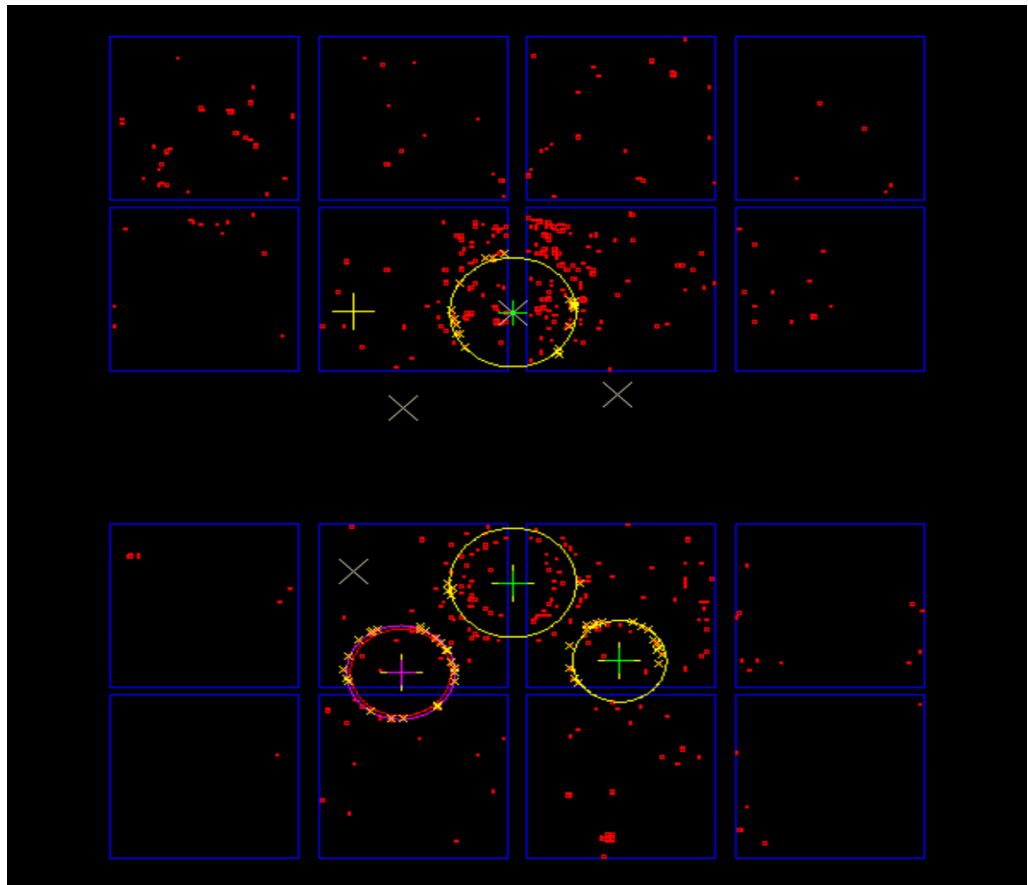


Figure 3.5: COMPASS RICH-1 detector – photon detection [9].

Optical system for upgrade RICH-1 detector

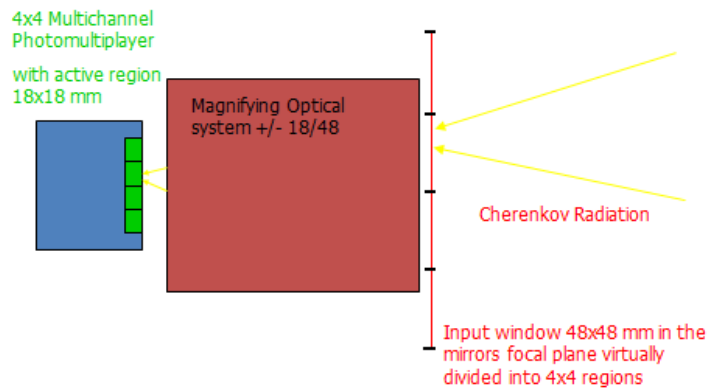


Figure 3.6: Optical system for RICH-1 upgrade with MCHPM [9].

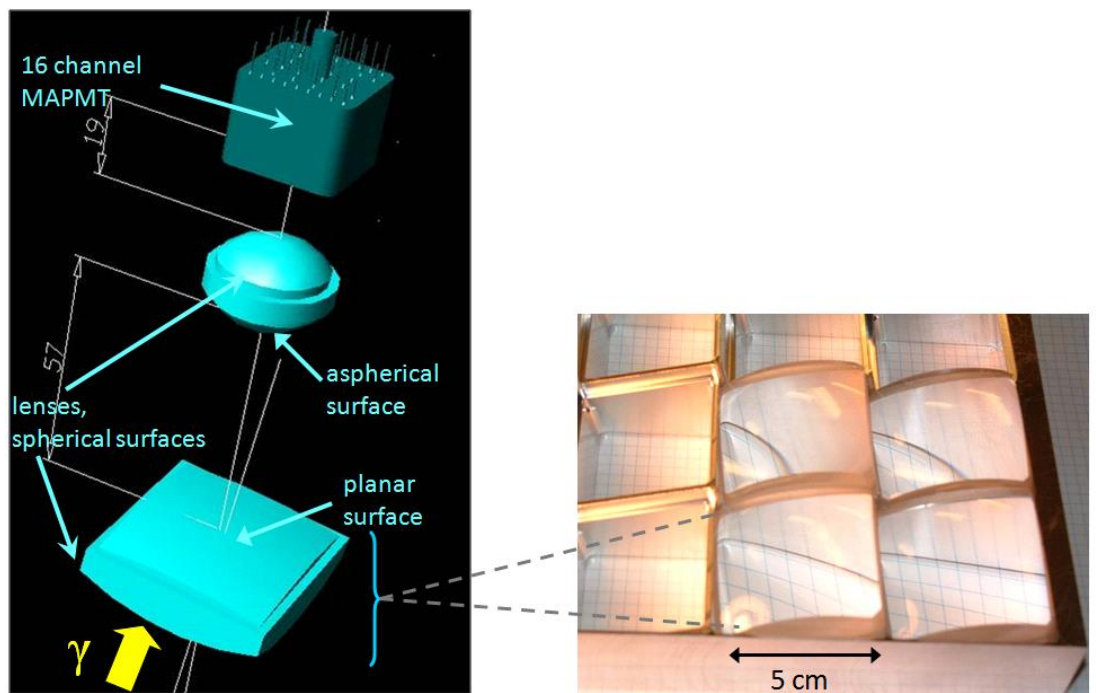


Figure 3.7: Optical telescopes for MCHPM [9].

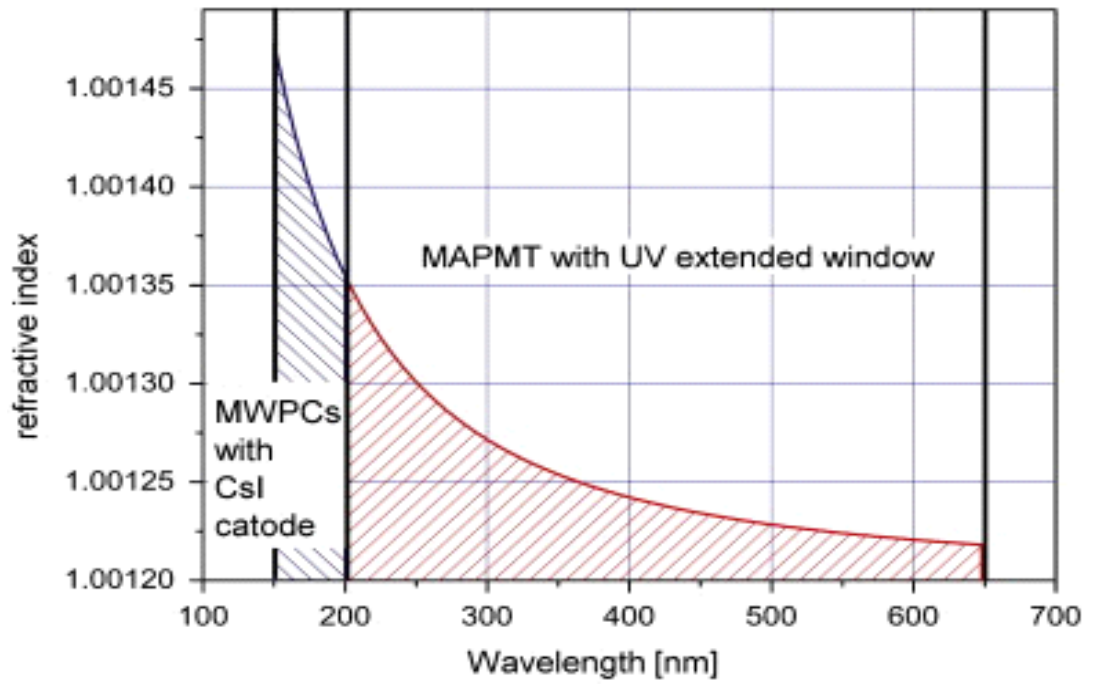


Figure 3.8: Dependence of refractive index of the C_4F_{10} on wavelength for MWPC and MAPMT [10].

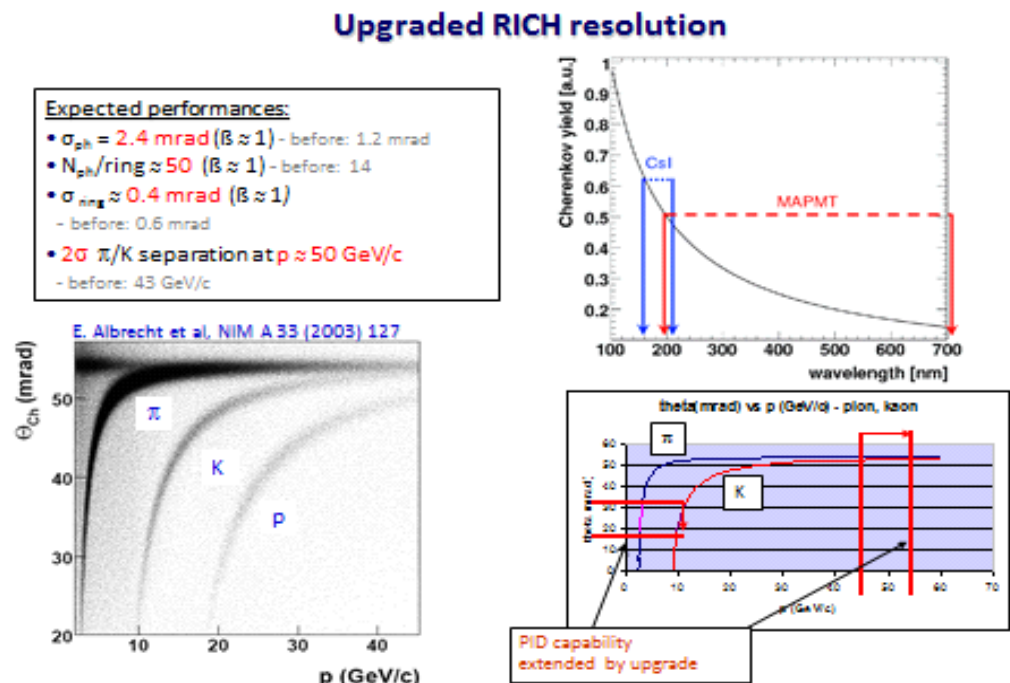


Figure 3.9: The upgraded by MCHPM RICH-1 resolution [9].

4 The hybrid photon detector based on THGEM and MicroMegas

The research and development programme (R&D) for the next upgrade of COMPASS RICH-1 photon detector system started in 2014 and it focuses on replacing at least a part of the remaining RICH-1 MWPC by a suitable photon hybrid detector based on bulk MicroMegas (Micro-Mesh Gaseous Structure) and THGEM (THick Gaseous Electron Multiplier) detectors.

4.1 The MicroMegas detector

As a suitable photon detector for the RICH upgrade the hybrid detector based on one bulk MicroMegas and two THGEM detectors is being developed.

The MicroMegas detector is a gaseous particle detector coming from the development of wire chambers. Invented in 1992 [11] by Georges Charpak and Ioannis Giomataris and further developed at CEA Saclay and CERN to provide stable, reliable and fast detectors the MicroMegas detectors are very suitable for the detection of ionising particles. The working principle of MicroMegas detector is shown in Figure 4.1.

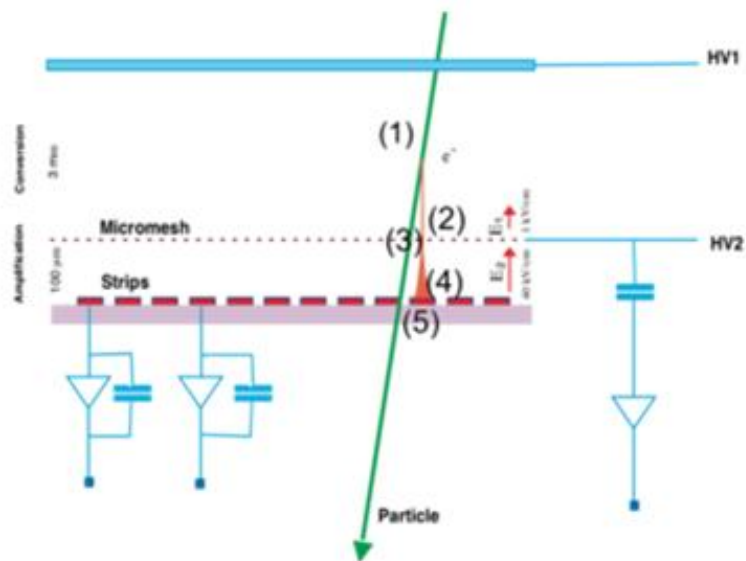


Figure 4.1.: The working principle of MicroMegas detector [12].

The MicroMegas detector detects particles by amplifying the charges that have been created by ionisation in the gas volume. In the MicroMegas detector, this gas volume is divided in two by a metallic micro-mesh between the read out electrodes. The micro-mesh is a key element of MicroMegas detector since it allows, at the same time, a high gain of about 10^4 and a fast signal of about 100 ns. In 2001, twelve large MicroMegas detector planes $40 \times 40 \text{ cm}^2$ were used for the first time at COMPASS for tracking purposes. Further example of the development of MicroMegas detectors is the invention of the “bulk” MicroMegas technology. The “bulk” technology consists of the integration of the micro-mesh with the printed circuit board that carries the read out electronics in order to build a monolithic detector. Such detector is very robust and can be produced within an industrial process.

4.2 The THGEM development

Another part of the new hybrid photon detector for COMPASS upgrade is the gas-electron-multiplier (GEM) system (Figure 4.2). In particular the new thick gas electron multipliers

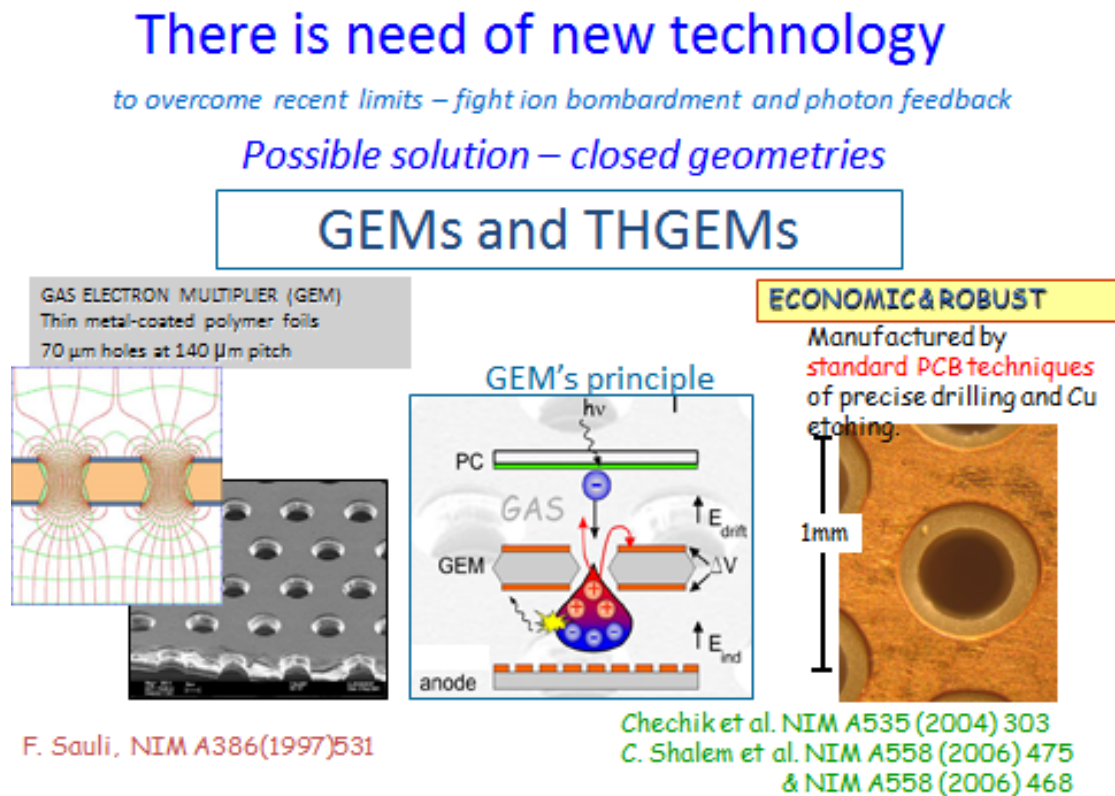


Figure 4.2: GEMs and THGEMs detectors

Electron's path

Ion's back-flow

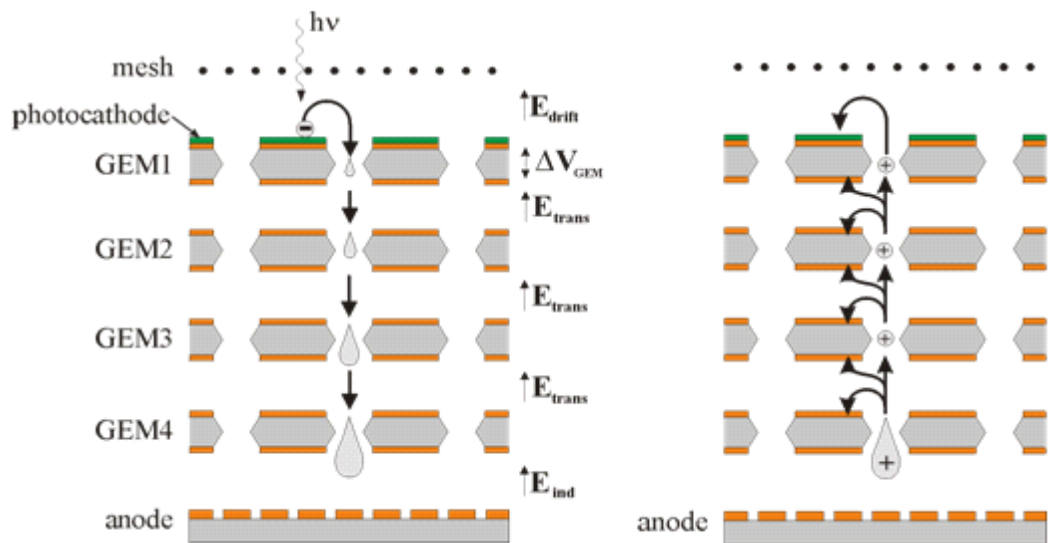


Figure 4.3: Multi GEMs detectors [9].

(THGEM) are being developed. The main motivation was that THGEMs provide potentially higher gain than GEMs. This R&D programme aimed to develop photon detectors based on multi-layer arrangements of thick GEM electron multipliers (Figure 4.3) coupled to a CsI photo converter. The thick GEMs have been characterised in detail including the study of the gain performance and the signal time evolution and their dependence on the geometrical parameters of the detector. The time-evolution features are exhibited by the gas detectors with open insulator surfaces. The variation due to this evolution dramatically depends on the THGEM parameters. The dedicated studies of the thick GEM gain and its evolution in time and their dependence on geometrical parameters have been experimentally studied.

4.3 Differences between GEM and THGEM

The THGEM is derived from GEM but it has different geometrical parameters. The scheme of the single-layer THGEM detector is shown in Figure 4.4.

Cu-coated polyimide foil is replaced by printed circuit boards (PCB), the holes are drilled. THGEM's holes are surrounded by a metal ring which is made by Cu-etching. This rim influences noticeably multiplier's features as will be shown in the next section. You can see the geometric arrangement in Figure. 4.5.

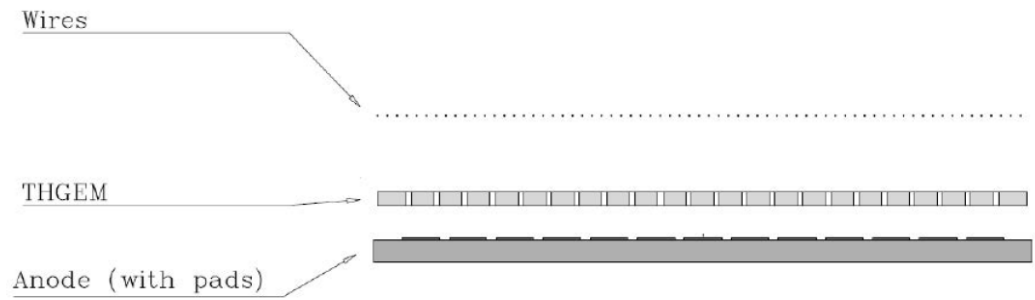


Figure 4.4: Scheme of the single-layer THGEM detector [12].

Last studies show rigorously the dependence of THGEM performance features and their time-evolution on THGEM geometrical parameters. For finding the methods how to reduce possible instabilities and fluctuations of the detector performance to the minimum, it is very important to understand these dependences.

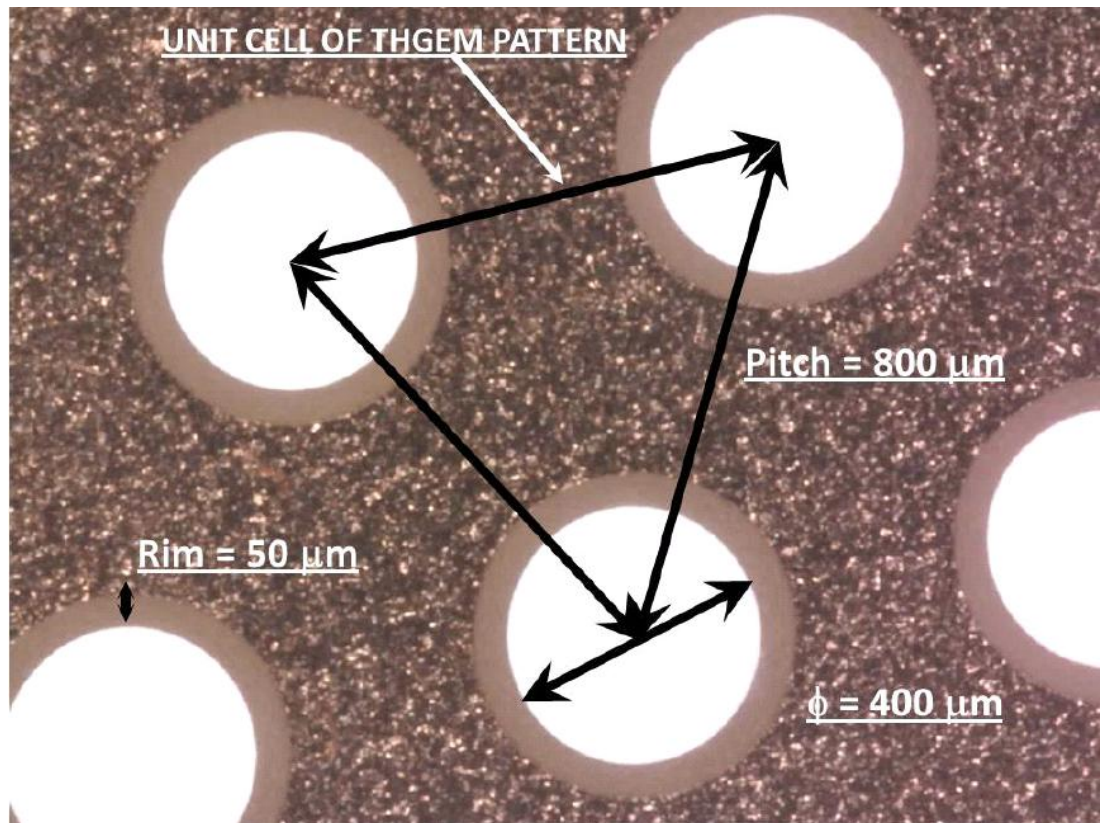


Figure 4.5: Detail of the THGEM printed-circuit board [12].

One of the differences between GEM and THGEM is the rim which surrounds holes in THGEM pattern. It was found that the rim about $100\ \mu\text{m}$ wide raises the gain to very high levels. The investigation of this dependence and the influence of the THGEMs thickness was made at a single layer detector. It was tested using X-rays.

The plane of wires creates an electric drift field, which concentrates electrons into the holes - most of electron multiplication takes place there. Then these electrons impact an anode, which is segmented to pads where the signal is collected. Two electrodes – THGEM-top (cathode) and THGEM-bottom (anode) are also a part of THGEM, so some electrons impact to THGEM-bottom and they don't participate on gain.

4.4 The THGEM gain time-evolution

Time evolution of the gain consists of two parts. The short-term part was noticeable in a range of minutes and the long-term part was measurable in a range of days. You can see an example of the short-term time evolution in Figure 4.6.

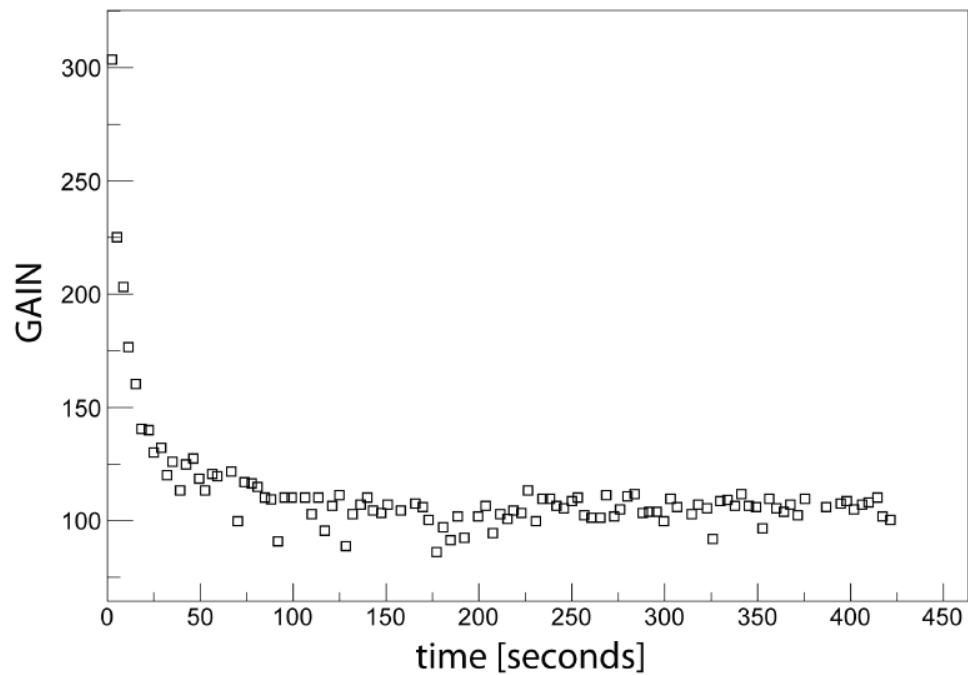


Figure 4.6: Short term time evolution of the THGEM gain [12].

The short-term effect appears because of presence of open dielectric surfaces. The charge, which is accumulated on the open surfaces, causes the difference in the electric field distribution and results in gain reduction. The time progress of the gain depends on the quantity of the surfaces, on the radiation volume and on the voltage. If the bias voltage level is high, the redundant charge on dielectric surfaces can lead to discharges during the start of the measuring process. The long-term time-evolution leads to discharges, which complicates the measurements.

The THGEM with a big rim was used because it gives bigger gain than multipliers without a rim or with a small rim – less than 20 μm . It was found that the gain of THGEMs with a big rim increases in time in contrast to THGEMs with a small rim or without a rim, where the gain decreases. You can see an example on Figure 4.7.

The short-time evolution has been investigated in two cases – the detector had been running ten hours when it was irradiated; the detector was one day off and then was irradiated when switching on. In the first case the gain was approximately ten times higher than in the second case for the large-rim THGEM. In comparison with the previous dependence, the no-rim THGEM gain dependence for the described states was negligible, as you can see in the Figure 4.8.

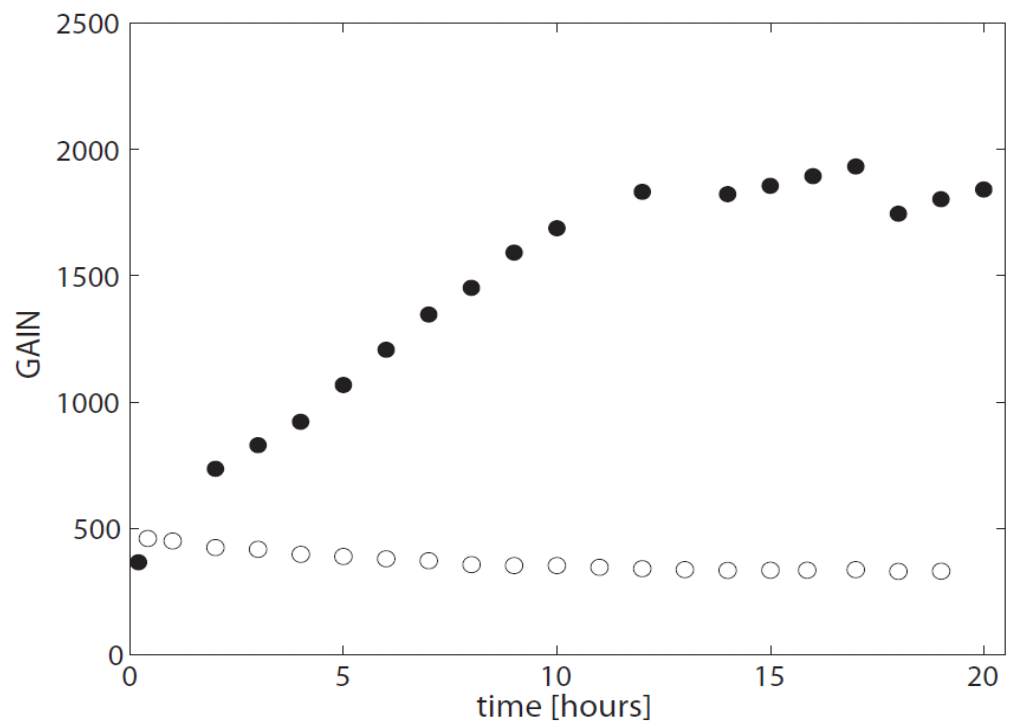


Figure 4.7.: Long-term time-evolution of the gain of THGEM continuous detector irradiation. (Black circles show THGEM with 100 μm width of rim and bias voltage 1750 V, white circles show no-rim THGEM on bias voltage 1330 V [12].

Measurement of anode current (Figure 4.9) revealed that the time-instability of large-rim THGEM is connected to its geometrical properties and it is not related to different gains or voltages.

These and other measurements, such as amplitude spectral investigation have shown, that large-rim THGEMs are not suitable, especially where the gain time-stability is needed. To achieve bigger gain it is possible to increase the THGEM thickness instead of a rim presence, but the bigger thickness is bonding with stronger electric field which can cause higher possibility of electric discharges.

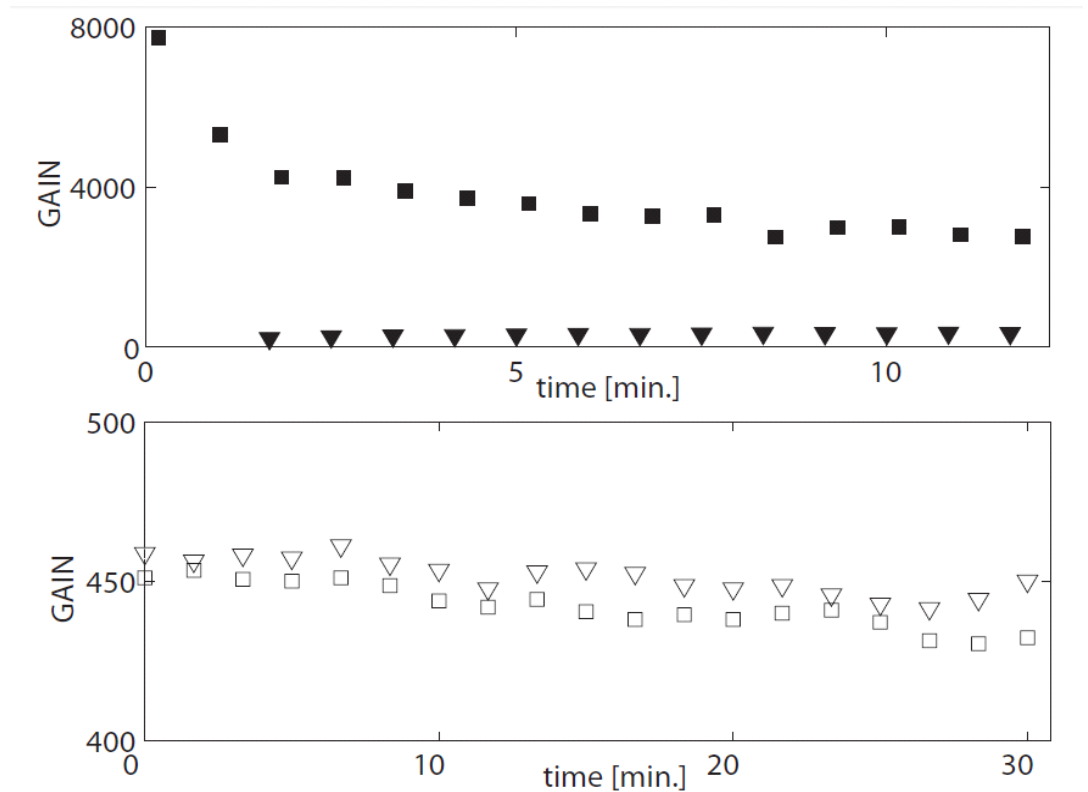


Figure 4.8: Fast time gain evolution. Black colour corresponds to 100 μm rim THGEM, white colour corresponds to no-rim THGEM. Squares correspond to measurement without previous irradiation triangles correspond to measurement after one day detector inactivity [12].

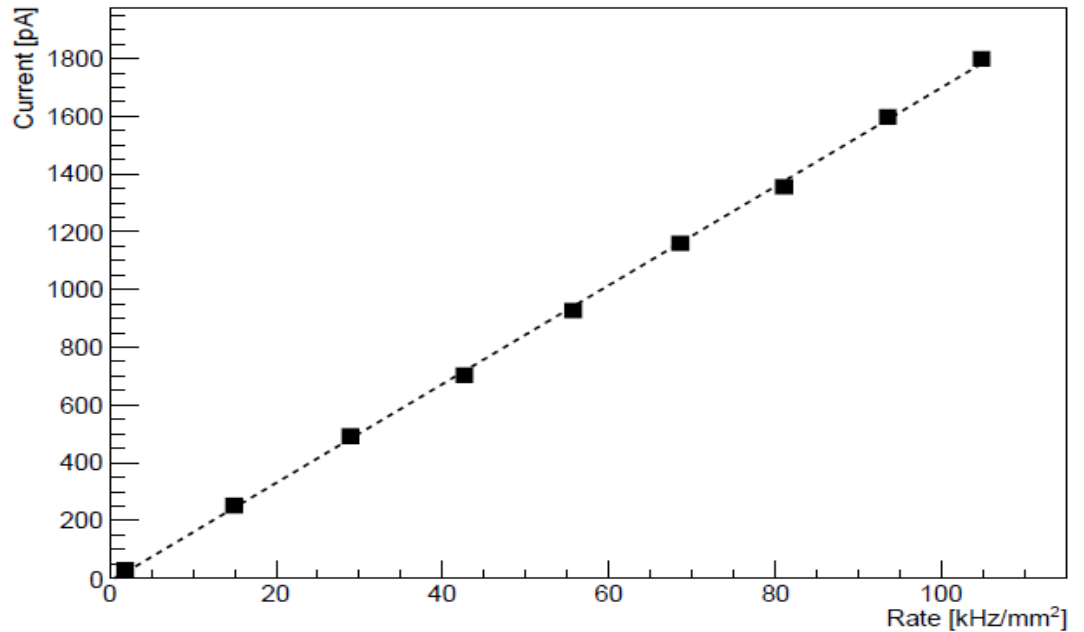


Figure 4.9: Anode current of the THGEM [12].

4.5 The hybrid photon detector prototype for COMPASS RICH-1 upgrade

Taking into account the results, described in sections 4.1 – 4.4, concerning the development of the photon detectors for the COMPASS RICH-1 upgrade to replace some of the present COMPASS RICH MWPC, the efforts were concentrated on the research and development of a suitable photon hybrid detector based on bulk MicroMegas and THGEM detectors.

The prototype of hybrid photon detector of the size 300 x 300 mm², consisting of one bulk MicroMegas and two THGEM detectors was prepared and tested. The MicroMegas was of the standard type, developed for COMPASS tracking. The micromesh had 12 x 12 mm² anodic pad and the resistive/capacitive anode at the ground. Each of the two THGEM had thickness 0.4 mm, the hole diameter 0.4 mm, the pitch equal 0.8 mm and no rim. The first THGEM has CsI

photon converting layer coating. The two THGEMs were positioned so to provide hole staggering which leads to lower charge density and higher mechanical stability.

The structure of the 300 x 300 mm² hybrid photon detector prototype for COMPASS RICH-1 upgrade is shown in Figure 4.10.

The Cherenkov light for photon detector prototype testing was produced by a 5 GeV π^- beam passing through the testing stand with the Cherenkov light radiator as shown in Figure 4.11.

The CERN T10 test beam area infrastructure with the 5 GeV π^- beam was used for our testing programme in August 2014. The gas mixture of 30% Ar and 70% CH₄ was used in the hybrid detector. The components of the hybrid detector were produced and assembled by Trieste group. Preliminary tests of the detector prototype before coating the first THGEM by CsI was done in the laboratory in Trieste with ⁵⁵Fe. The standard read out chain used for RICH-1 MAPMP configuration was used also for our testing of hybrid photon detector prototype. Front end electronic, digitalization and control components used were developed by Turin and Freiburg COMPASS groups and DAQ system used was developed by Munich and Prague COMPASS groups. The wavelength range of detected Cherenkov light registered by the hybrid detector prototype with CsI coated THGEM is shown in Figures 3.8 and 3.9.

The obtained single Cherenkov photon amplitude spectra from the 300 x 300 mm² hybrid photon detector are shown in Figure 4.12 and the time resolution spectra in Figure 4.13.

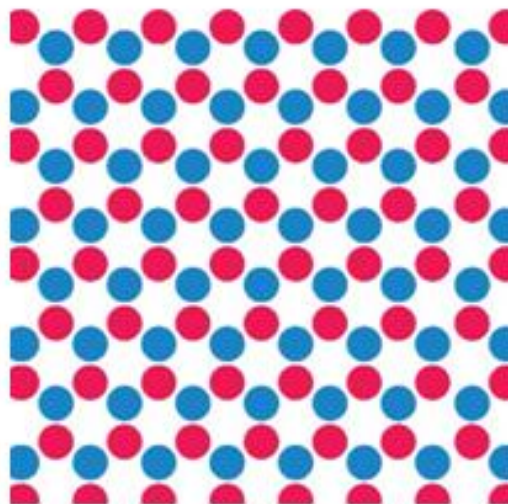
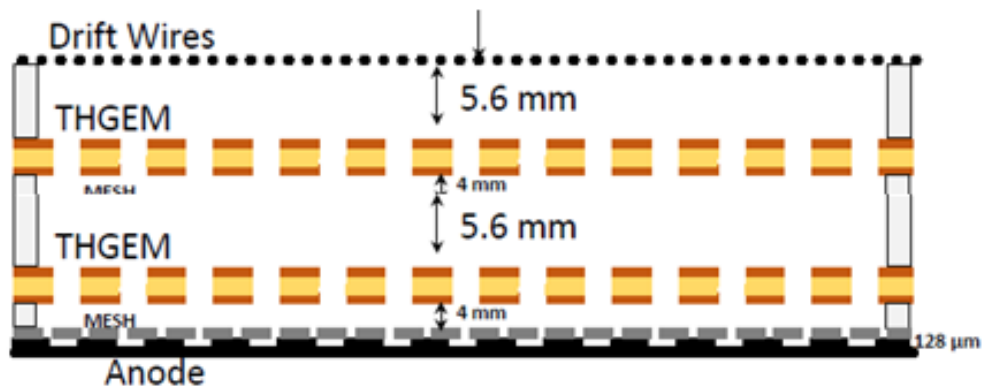


Figure 4.10: Structure of the $300 \times 300 \text{ mm}^2$ hybrid photon detector for COMPASS RICH-1 upgrade consisting of one MicroMegas and two THGEM detectors [13].

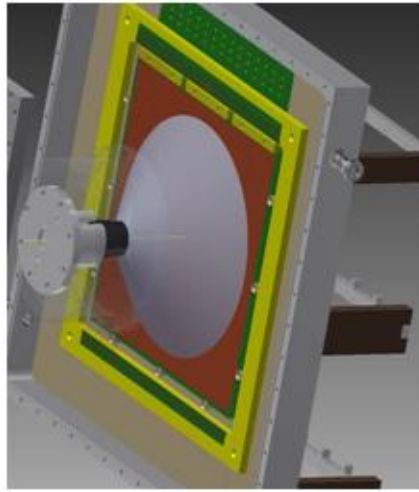


Figure 4.11: Testing stand at CERN SPS 5 GeV pi(-) beam of the 300 x 300 mm² hybrid photon detector for COMPASS RICH-1 upgrade consisting of one MicroMegas and two THGEM detectors [13].

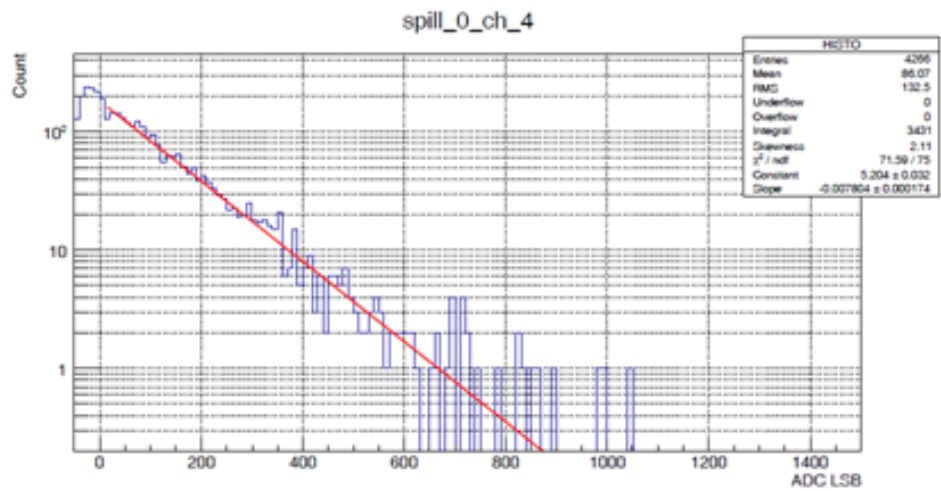


Figure 4.12: Single Cherenkov photon amplitude spectra of the 300 x 300 mm² hybrid photon detector for COMPASS RICH-1 upgrade consisting of one MicroMegas and two THGEM detectors [13].

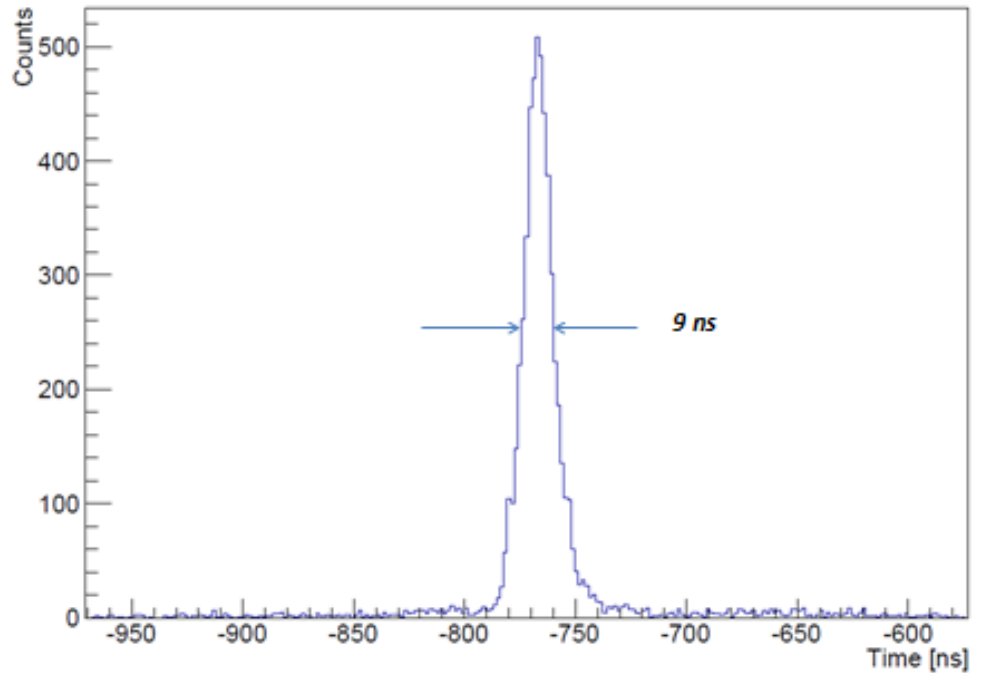


Figure 4.13: Time resolution of the $300 \times 300 \text{ mm}^2$ hybrid photon detector for COMPASS RICH-1 upgrade consisting of one MicroMegas and two THGEM detectors [13].

4.6 Possible future direction of research

Taking into account the present achievements in testing of the hybrid photon detector prototype, the work to prepare photon detectors based on one MicroMegas and two THGEM detectors and corresponding detector readout to replace in 2016 four MWPC of the COMPASS RICH-1, as indicated in Figure 4.14, is going on.

The development and production of the photon detector with large THGEM active area size of $600 \times 600 \text{ mm}^2$ is a challenge for the upcoming years. The necessity to ensure a uniform response of such detectors requires the use of top level production technology.

For successful upgrade of the COMPASS RICH-1 photon detector, further studies of THGEM's performance and its dependence on geometrical arrangement of the detector are necessary. It especially concerns the performance of no-rim THGEMs or the THGEMs with a small rim.

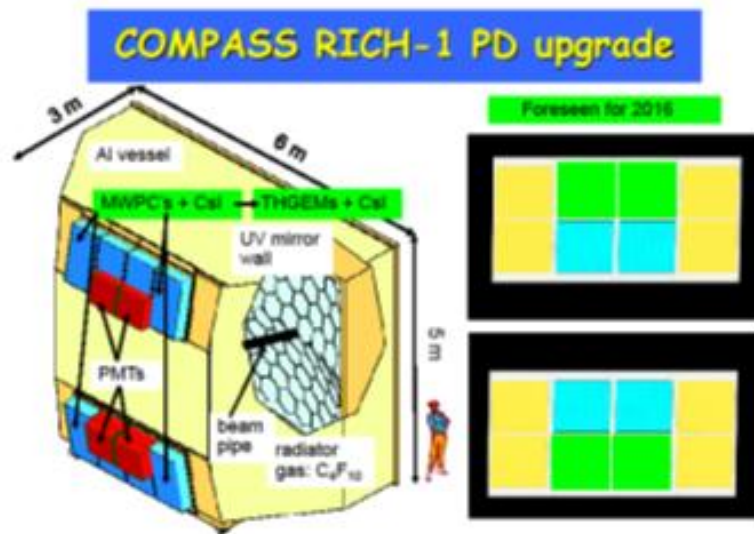


Figure 4.14: COMPASS RICH-1 photon detector upgrade foreseen for 2016 [13].

Conclusion

In this thesis we demonstrated the importance of a large fast gaseous Ring Imaging Cherenkov Detector for high quality hadron identification in the broad range of energies at COMPASS experiment. The Cherenkov radiation and the principles of Ring Imaging Cherenkov detection for particle identification as well as its use at COMPASS are described in details.

The thesis is a part of the research and development programme (R&D) aiming at the next upgrade of COMPASS RICH-1 photon detector system and is focused on the replacing at least a part of the present RICH-1 Multi Wire Proportional Chambers (MWPC) detectors of Cherenkov radiation by a suitable photon hybrid detectors based on the bulk Micro-Mesh Gaseous Structure detectors (MicroMegas) coupled to the Thick Gas Electron Multiplier (THGEM) with CsI photon convertor.

The prototype of a novel hybrid photon detector of the size $300 \times 300 \text{ mm}^2$, consisting of one bulk MicroMegas and two THGEM detectors, the first one with CsI photon convertor coating, was prepared and tested.

In the ongoing R&D programme special attention was dedicated both to establish the principles and to develop the engineering aspects of detectors of single photons based on multi-layer arrangement of THGEMs coupled to a CsI photo converting coating. The THGEM gain has been studied in details including its dependence on the THGEM geometrical parameters and its time-evolution. These THGEM features are important for the development of such novel detectors and the time evolution of the detector gain has to be known in detail in order to evaluate and minimise its impact on the quality of the physics data registered in experiments.

The data concerning the THGEM gain dependence on a rim presence and size and the THGEM thickness have been obtained. The time evolution of the gain has been analysed in detail. The provided experimental evidence clearly indicates that the use of large rim THGEMs must be avoided, at least for all applications that require stable detector gain. Moreover, when the complete collection of the free

electrons is critical, as it is the case of photon detectors where the efficiency depends on the detection of single photoelectrons, this choice is inevitable.

The performed tests of the developed 300 x 300 mm² hybrid photon detector prototype consisting of one MicroMegas and two THGEM detectors showed, that such a detector is very reliable in operation, achieving steady gain about 130 thousands and time resolution of about 9 ns. Both components of the hybrid detector – the MicroMegas as well as THGEM are very robust and can be produced within an industrial process.

Bibliography

- [1] *COMPASS* [online]. [cit. 2015-04-05]. Available from: <http://wwwcompass.cern.ch/>
- [2] *CERN* [online]. [cit. 2015-04-05]. Available from: <http://home.web.cern.ch/about>
- [3] *Group for Cooperation with CERN* [online]. [cit. 2015-06-02]. Available from: <http://physics.mff.cuni.cz/kfnt/cern/?page=gallery>
- [4] H. Alaeian. *An Introduction to Cherenkov Radiation* [online]. [cit. 2015-05-02]. Available from: <http://large.stanford.edu/courses/2014/ph241/alaeian2/>
- [5] P. Nahin, *Oliver Heaviside, sage in solitude: the life, work, and times of an electrical genius of the Victorian age* [online]. : 26-0911-26-0911 [cit. 2015-05-23]. DOI: 10.5860/choice.26-0911.
- [6] J. Hrubý, *Čerenkovo záření* [online]. [cit. 2015-05-01]. Available from: <http://www.pf.jcu.cz/stru/katedry/fyzika/prof/Svadlenkova/Cerenkovovo%20zareni.pdf>
- [7] J. Kvasnica, *Teorie Čerenkovova záření. (Czech) (Theory of Cherenkov radiation)*, Pokroky matematiky, fyziky a astronomie, 4 (1959) No. 3, 302--308
- [8] *Maxwell's Equations* [online]. [cit. 2015-05-23]. Available from: <http://www.maxwells-equations.com/>
- [9] M. Finger, Osaka, APSE2010, June 17, 2010
- [10] P. Abbon et al., Design and construction of the fast photon detection system for COMPASS RICH-1. *Nuclear Instruments and Methods in Physics Research Section A: Accelerators, Spectrometers, Detectors and Associated Equipment*, NIMA 616(1) (2010) 21-37

- [11] Nuclear Instruments and Methods in Physics Research Section A: Accelerators, Spectrometers, Detectors and Associated Equipment Volume 376, Issue 1, Pages 29-35 (21 June 1996)
- [12] M. Alexeev, et al. The gain in Thick GEM multipliers and its time-evolution. *Journal of Instrumentation* [online]. 2015, **10**(03): P03026-P03026 [cit. 2015-06-02]. DOI: 10.1088/1748-0221/10/03/p03026.
- [13] F- Tessarotto. *Outcome from the test beam for the RICH upgrade COMPASS* [online]. CERN, 2014. Available from: http://wwwcompass.cern.ch/compass/collaboration/2014/co_1409/pdf/tessarotto_250925.pdf
- [14] P. Abbon et al., The Compass Experiment at CERN , NIMA 577 (2007) 455-518
- [15] Compass Collaboration: The Comoass II Proposal, CERN-SPSC-2010-014, SPSC-P-340
- [16] P. Abbon et al., Fast photon detection for COMPASS RICH-1, NIMA 572 (2007) 419-421
- [17] P. Abbon et al., The COMPASS RICH-1 detector upgrade, EPJ ST 162 (2008) 251-257
- [18] G. Alexeev et al., Detection of single photons with THGEM-based counters, NIMA 695(2012)159-162

List of Figures

Figure 1.1: COMPASS setup in 2014

Figure 1.2: COMPASS spectrometer in 2014

Figure 2.1: Spreading wave scheme A

Figure 2.2: Spreading wave scheme B

Figure 2.3: Spreading wave scheme C

Figure 2.4: Angle of interference scheme

Figure 3.1: COMPASS RICH-1 detector – photon detection

Figure 3.2: COMPASS RICH-1 detector – schematic view

Figure 3.3: Particle identification with COMPASS RICH-1

Figure 3.4: COMPASS RICH-1 detector – mirror system and photon detection

Figure 3.5: COMPASS RICH-1 detector – photon detection

Figure 3.6: Optical system for RICH-1 upgrade with MCHPM

Figure 3.7: Optical telescopes for RICH-1 upgrade with MCHPM

Figure 3.8: Dependence of refractive index of the C_4F_{10} on wavelength for MWPC and MAPMT.

Figure 3.9: The upgraded by MCHPM RICH-1 resolution

Figure 4.1: Working principle of MicroMegas detector

Figure 4.2: GEMs and THGEMs detectors

Figure 4.3: Multi GEMs detectors

Figure 4.4: Scheme of the single-layer THGEM detector

Figure 4.5: Detail of the THGEM printed-circuit board

Figure 4.6: Short term time evolution of the THGEM gain

Figure 4.7: Long term time evolution of the THGEM gain

Figure 4.8: Fast time evolution of the THGEM gain

Figure 4.9: Anode current of the THGEM

Figure 4.10: Structure of the $300 \times 300 \text{ mm}^2$ hybrid photon detector for COMPASS RICH-1 upgrade consisting of one MicroMegas and two THGEM detectors

Figure 4.11: Testing stand at CERN SPS 5 GeV $\pi(-)$ beam of the $300 \times 300 \text{ mm}^2$ hybrid photon detector for COMPASS RICH-1 upgrade consisting of one MicroMegas and two THGEM detectors

Figure 4.12: Single Cherenkov photon amplitude spectra of the $300 \times 300 \text{ mm}^2$ hybrid photon detector for COMPASS RICH-1 upgrade consisting of one MicroMegas and two THGEM detectors

Figure 4.13: Time resolution of the $300 \times 300 \text{ mm}^2$ hybrid photon detector for COMPASS RICH-1 upgrade consisting of one MicroMegas and two THGEM detectors

Figure 4.14: COMPASS RICH-1 photon detector upgrade foreseen for 2016

List of Abbreviations

COMPASS – Common Muon and Proton Apparatus for Structure and Spectroscopy

CERN – Conseil Européen pour la Recherche Nucléaire

SPS – Super Proton Synchrotron

PID – Particle identification

RICH – Ring Imaging Cherenkov counter

MWPC – Multi Wire Proportional Chambre

MAPMT – Multi Anode Photomultiplier Tube

TDC – Time-to-Digital Convertor

ADC – Analog-to-Digital Convertor

GEM – Gas Electron Multiplier

THGEM – Thick Gas Electron Multiplier

LAS – Large Angle Spectrometer

SAS – Small Angle Spectrometer

CDR – Central Data Recording

DC – Data Collection

DAQ – Data Acquisition

MW – Muon Wall

ECAL – Electromagnetic Calorimeter

HCAL – Hadron Calorimeter

UV – Ultra Violet

PMT – Photo Multiplier Tube

R&D – Research and Development